Plasticity in the Meiotic Epigenetic Landscape of Sex Chromosomes in *Caenorhabditis* Species

Braden J. Larson,[1,2] Mike V. Van,[1] Taylor Nakayama, and JoAnne Engebrecht[3]
Department of Molecular and Cellular Biology, University of California, Davis, California 95616
ORCID ID: 0000-0002-2733-7506 (J.E.)

ABSTRACT During meiosis in the heterogametic sex in some species, sex chromosomes undergo meiotic sex chromosome inactivation (MSCI), which results in acquisition of repressive chromatin and transcriptional silencing. In *Caenorhabditis elegans*, MSCI is mediated by MET-2 methyltransferase deposition of histone H3 lysine 9 dimethylation. Here we examined the meiotic chromatin landscape in germ lines of four *Caenorhabditis* species; *C. remanei* and *C. brenneri* represent ancestral gonochorism, while *C. briggsae* and *C. elegans* are two lineages that independently evolved hermaphroditism. While MSCI is conserved across all four species, repressive chromatin modifications are distinct and do not correlate with reproductive mode. In contrast to *C. elegans* and *C. remanei* germ cells where X chromosomes are enriched for histone H3 lysine 9 dimethylation, X chromosomes in *C. briggsae* and *C. brenneri* germ cells are enriched for histone H3 lysine 9 trimethylation. Inactivation of *C. briggsae* MET-2 resulted in germ-line X chromosome transcription and checkpoint activation. Further, both histone H3 lysine 9 di- and trimethylation were reduced in *Cbr-met-2* mutant germ lines, suggesting that in contrast to *C. elegans*, H3 lysine 9 di- and trimethylation are interdependent. *C. briggsae* H3 lysine 9 trimethylation was redistributed in the presence of asynapsed chromosomes in a sex-specific manner in the related process of meiotic silencing of unsynapsed chromatin. However, these repressive marks did not influence X chromosome replication timing. Examination of additional *Caenorhabditis* species revealed diverse H3 lysine 9 methylation patterns on the X, suggesting that the sex chromosome epigenome evolves rapidly.

KEYWORDS genetics of sex; histone methyltransferases; meiosis; MSCI; MSUC; sex chromosomes

SEXUAL reproduction relies on the specialized cell division program of meiosis for the generation of haploid gametes. During meiosis, an elaborate chromosome dance occurs where chromosomes pair side by side, synapse via the elaboration of the synaptonemal complex (SC), a tripartite proteinaceous structure, and undergo crossover recombination to connect homologous chromosomes, thus ensuring that homologs segregate from each other at the first meiotic division (reviewed in Zickler and Kleckner 2015). Defects in chromosome pairing, synapsis, or recombination can lead to infertility or aneuploid progeny, and thus it is critical that germ cells monitor these events and ensure they occur properly. However, sex chromosomes of the heterogametic sex are either partially (*e.g.*, XY in mammalian and *Drosophila* males) or completely hemizygous (*e.g.*, X0 in a number of insects and worms). Consequently, sex chromosomes, or the underlying meiotic program, must be modified to promote sex chromosome segregation during meiosis.

Meiotic sex chromosome inactivation (MSCI) is the process whereby sex chromosomes accumulate repressive chromatin marks and are transcriptionally silenced (Handel 2004) and has been proposed to be important for sex chromosome transmission during meiosis (reviewed in Checchi and Engebrecht 2011b and Turner 2015). MSCI has been reported to occur in diverse species, including *Caenorhabditis elegans* (Kelly *et al.* 2002) and *Homo sapiens* (de Vries *et al.* 2012). In *C. elegans*, MSCI is important for shielding the hemizygous X from checkpoint machinery (Checchi and Engebrecht 2011a). On the other hand, elegant work by Turner and colleagues has demonstrated that MSCI is essential for preventing the expression of a small number of Y-linked genes during male

doi: 10.1534/genetics.116.191130
Manuscript received April 30, 2016; accepted for publication June 6, 2016; published Early Online June 8, 2016.
Supplemental material is available online at www.genetics.org/lookup/suppl/doi:10.1534/genetics.116.191130/-/DC1.
[1]These authors contributed equally to this work.
[2]Present address: Molecular, Cell and Developmental Biology, University of California, Santa Cruz, CA 95064.
[3]Corresponding author: Department of Molecular and Cellular Biology, 1 Shields Ave., University of California, Davis, CA 95616. E-mail: jengebrecht@ucdavis.edu

meiosis in mice (Royo *et al.* 2010). Further, the conservation of MSCI has recently been brought into question, as chickens do not appear to undergo MSCI even though they have differentiated sex chromosomes (Guioli *et al.* 2012), and in *Drosophila*, the topic has been highly debated (Vibranovski *et al.* 2009; Meiklejohn *et al.* 2011; Mikhaylova and Nurminsky 2011; Vibranovski 2014). Thus, the universality and precise role of MSCI is not currently known.

MSCI has been proposed to be related to, and evolved from, the more general silencing that occurs when any unpaired chromatin is present, termed meiotic silencing of unpaired or unsynapsed chromatin (MSUC) (Maine *et al.* 2005; Schimenti 2005). However, at least in worms, evidence exists that these processes are not identical and may involve different molecular machinery (Checchi and Engebrecht 2011a). In mice, the tumor suppressor, BRCA1 has been shown to be required for both MSCI and MSUC through recruitment of the checkpoint kinase ATR (Turner *et al.* 2004, 2005); however, the precise molecular pathway(s) for acquisition of either MSUC or MSCI has not been elucidated.

While reproductive strategies, and sex chromosomes, have evolved independently in many different lineages, the process of meiosis is well conserved. This is illustrated by the robust conservation of the meiotic recombination machinery (Villeneuve and Hillers 2001; Cole *et al.* 2010). On the other hand, components of the SC are less conserved; however, analyses in the basal metazoan hydra suggests that there is a higher level of conservation of SC components than previously thought (Fraune *et al.* 2012). Information about the conservation of the molecular machinery that mediates MSCI or MSUC is more limited.

Here we examined meiotic silencing in the *elegans* group of nematodes, which includes both female/male and independently evolved hermaphroditic/male species (reviewed in Ellis and Lin 2014). These worms are morphologically very similar, yet recent studies indicate that the genetic networks underlying these similarities have diverged substantially (Verster *et al.* 2014). We found that while MSCI and MSUC are conserved among this group of worms, the repressive chromatin marks that mediate these processes and their regulatory gene networks are distinct, suggesting significant plasticity in the sex chromosome epigenetic landscape.

Materials and Methods

Genetics

Strains were maintained at 20° unless otherwise noted. *C. elegans* var. Bristol (N2), *C. briggsae* (AF16), *C. remanei* (SB146), *C. brenneri* (CB5161), *C. sinica* (JU1201), *C. nigoni* (JU1325), *C. latens* (VX88), *C. wallacei* (JU1873), *C. tropicalis* (JU1373), *C. doughertyi* (JU1333), and *C. japonica* (DF5081) were used as the wild-type (WT) strain for each respective species. *C. briggsae* RNA interference (RNAi) sensitive by feeding strain JU1018:*mfIs42*[*Cel-sid-2* + *Cel-myo-2*::DsRed] was generated by Nuez and Felix (2012). Some nematode strains used in this work were provided by the *Caenorhabditis* Genetics Center, which is funded by the National Institutes of Health (NIH) National Center for Research Resources.

Cytological analysis

Immunostaining of germ lines was performed as described (Jaramillo-Lambert *et al.* 2007), with the following alterations for anti-phospho-Chk1(Ser345): The gonads were blocked with 0.7% BSA in PBS 0.2% Triton for 1 hr; slides were incubated overnight at 4° in a humidifying chamber. The following primary antibodies were purchased and used at the indicated dilutions: mouse anti-histone H3K4me2 (1:500; catalog no. 05-1338), rabbit anti-histone H3K9me2 (1:500; catalog no. 07-441), rabbit anti-histone H3K9me3 (1:500; catalog no. 07-442) (Millipore, Temecula, CA), mouse anti-histone H3K9me2 (1:500; catalog no. ab1220), rabbit anti-Pol2 Ser2-P (1:500; catalog no. ab5095), mouse anti-Pol2 Ser5-P (1:500; catalog no. ab5408) (Abcam, Cambridge, MA), and rabbit anti-phospho-Chk1(Ser345) (1:50; catalog no. sc-17922) (Santa Cruz Biotechnology, Santa Cruz, CA). Goat anti-SYP-1 (1:250) and rabbit anti-SYP-2 (1:250) were generous gifts from Sarit Smolikove (University of Iowa) and generated using VDAPTEALIETPVDDQSSGFLC (*Cel*-SYP-1) and SSLKKRPGPQDDRRC (*Cel*-SYP-2) peptide sequences. The following secondary antibodies from Life Technologies were all used at 1:500 dilutions (except for with pCHK-1 staining, where secondary was used at 1:250): Alexa Fluor 594 goat anti-mouse IgG, Alexa Fluor 488 goat anti-mouse IgG, Alexa Fluor 555 goat anti-rabbit IgG, Alexa Fluor 488 goat anti-rabbit IgG, and Alexa Fluor 488 donkey anti-goat IgG. DAPI (2 μg/ml; Sigma-Aldrich, St. Louis, MO) was used to counterstain DNA.

Collection of images was performed using an API Delta Vision deconvolution microscope or Nikon Instruments Eclipse Ti-E microscope. A minimum of three germ lines were examined for each condition and experiments were repeated a minimum of three times. Images were deconvolved using Applied Precision SoftWoRx or Huygens imaging analysis software, respectively, and subsequently processed and analyzed using Fiji (ImageJ) (Wayne Rasband, NIH). Pixel intensity values for each nucleus were calculated by Fiji and then corrected for background signal by subtracting the mean background intensity. Phospho-CHK-1 foci that surpassed the default threshold value of 51 were counted manually using the cell counter plugin in Fiji. Student's *t*-tests were used to analyze data.

RNAi analysis

RNAi experiments were performed at 20°, using the feeding method (Timmons *et al.* 2001). For *C. briggsae*, L4 hermaphrodites were mated with mix-staged males. After 24 hr, mated hermaphrodites were identified by the presence of a mating plug and transferred onto RNAi plates. The resulting progeny were then analyzed cytologically. *Cbr-met-2* sequences were isolated from AF16 genomic DNA and inserted

into the L4440 vector via restriction cloning. *Cbr-mes-2*, *Cbr-set-25*, *Cbr-him-8*, *Cbr-zim-2*, *Cbr-zim-1*, and *Cbr-chk-1* sequences were isolated from AF16 genomic DNA and inserted into the L4440 vector by Gibson assembly. Primers used for cloning are listed in Supplemental Material, Table S1. Previous analyses by Phillips and Dernburg (2006) identified the *C. briggsae him/zim* operon; we assigned the ORFs CBG12897 and CBG12895 as *Cbr-zim-2* and *Cbr-zim-1*, respectively, based on phenotypic analyses (see Figure 6). Cultures were plated onto NGM plates containing 25 μg/ml carbenicillin and 1 mM IPTG and were used within 2 weeks.

Clustered regularly interspaced short palindromic repeats/Cas9 generation of Cbr-met-2 mutants

Cbr-met-2 targeting sequences were inserted into the Cas9 + single guide RNA (sgRNA) vector pDD162 (*Peft-3*::Cas9 + Empty sgRNA) using the Q5 Site-Directed Mutagenesis Kit (New England Biolabs, Beverely, MA) with forward primer 5′-N_{19}GTTTTAGAGCTAGAAATAGCAAGT-3′, where N_{19} is replaced by the desired 19-bp targeting sequence, and reverse primer 5′-CAAGACATCTCGCAATAGG-3′ (Dickinson *et al*. 2013). The sgRNA sequences and corresponding protospacer adjacent motifs protospacer adjacent motifs (PAM) sites, indicated in parentheses, were: *Cbr-met-2* sgRNA#1 TCGAAGCAGTTGTATCCGG (GGG) and *Cbr-met-2* sgRNA#2 GGAGAAAATGGGAAAAAGG (AGG).

Plasmid mixtures were microinjected into the gonads of young adult *C. briggsae* hermaphrodites. Plasmids for injection were prepared using a Mini-Prep Plasmid Purification Kit (Qiagen, Valencia, CA; catalog no. 27106). To generate large deletions in the *Cbr-met-2* gene 50 ng/μl Cas9+*Cbr-met-2* sgRNA#1 and 50 ng/μl Cas9+*Cbr-met-2* sgRNA#2 vectors, and 5 ng/μl pCFJ90 (p*Cel-myo-2*:mCherry pharyngeal co-injection marker) were injected. After recovery, each worm was placed onto an individual OP50 plate. A total of 26 worms were injected, three of which laid at least one worm with a red pharynx.

Plates with singled injected worms (F_0) were screened for F_1 progeny with red pharynxes. F_1 worms from a plate with at least one glower were singled and allowed to lay eggs for 24 hr. The singled F_1 worms were then collected and lysed for PCR screening using primers outside of the sgRNA sequences. Deletion alleles were detected by the presence of smaller than WT bands in the PCR reaction. Primers used were as follows: *Cbr-met-2* deletion forward AGTGGCCA TAGGGGAGACTT; *Cbr-met-2* deletion external reverse, GTAAAGGACGTGCTGGACGA; *Cbr-met-2* deletion internal reverse, GTGGCATCGTTTTGACGGAC. Deletion alleles were then recovered, homozygosed, sequenced, and backcrossed two times. In total, 40 F_1 worms were screened by PCR and two deletion alleles were recovered.

Reagent and data availability

Strains generated in this study have been deposited in the *Caenorhabditis* Genetics Center. Complete imaging data sets are available upon request.

Results

The spatiotemporal organization of the germ line is conserved among Caenorhabditis species

The *C. elegans* germ line is an excellent model for investigating molecular mechanisms of meiosis; germ cells of the syncytial gonad are arranged in a stereotypical spatiotemporal pattern where all stages of meiotic prophase are visible (Lui and Colaiacovo 2013). At the distal end, germ cells divide mitotically [proliferative zone (PZ)] and as cells move proximally they enter meiotic prophase. During leptotene/zygotene, chromosomes pair and initiate synapsis resulting in crescent-shaped nuclei [transition zone (TZ)]. Progression along the gradient corresponds to the classic stages of pachytene (side-by-side alignment/synapsis of homologous chromosomes), diplotene (Dip) (desynapsis and chromosome condensation) and diakinesis (Dia) (continued condensation; the six bivalents connected by chiasmata are clearly visible) (Figure 1A). During oogenesis, meiotic prophase is coupled to cellular growth and oocytes arrest prior to the meiotic divisions, while during spermatogenesis, further chromosome condensation occurs and the haploid products of the meiotic divisions are packaged into sperm (MI, MII, sperm; Figure 1A) (Shakes *et al.* 2009). In hermaphrodites, the first wave of germ cells becomes sperm; as adults, hermaphrodites exclusively produce oocytes (reviewed in Hubbard and Greenstein 2005).

To determine the degree of conservation of the spatiotemporal organization of the germ line, we examined germ lines of four of the *elegans* group: the androdioecious species (hermaphrodites/males) *C. elegans* and *C. briggsae* and the gonochoristic species (female/male) *C. remanei* and *C. brenneri* (Kiontke and Fitch 2005; Kiontke *et al.* 2011). We found that the spatiotemporal organization of the germ line was similar in all of the species as visualized by DAPI staining (Figure 1B). Analysis of the individual stages revealed subtle differences in the percentage of nuclei found in the PZ, TZ, and pachytene (Figure S1). In hermaphrodites/females more pronounced differences were observed in diplotene/diakinesis; this included the number of oocytes observed once they formed a single row and a transient chromosome elongation phase in some species prior to condensation at diakinesis (Figure 1C). These differences correlate with genome size; the largest genome, *C. brenneri* (Fierst *et al.* 2015), had the longest diplotene/diakinesis stage and the most pronounced chromosome elongation (Figure 1C). Nonetheless, the overall structure and organization of the germ line is conserved among these *Caenorhabditis* species.

The X chromosome of males in both androdioecious and gonochoristic Caenorhabditis species is subject to MSCI

In many species where sex determination is chromosomally based, including *C. elegans*, sex chromosomes in germ cells of the heterogametic sex undergo MSCI, resulting in repressive chromatin and transcriptional silencing (reviewed in Checchi and Engebrecht 2011b and Turner 2015). To determine

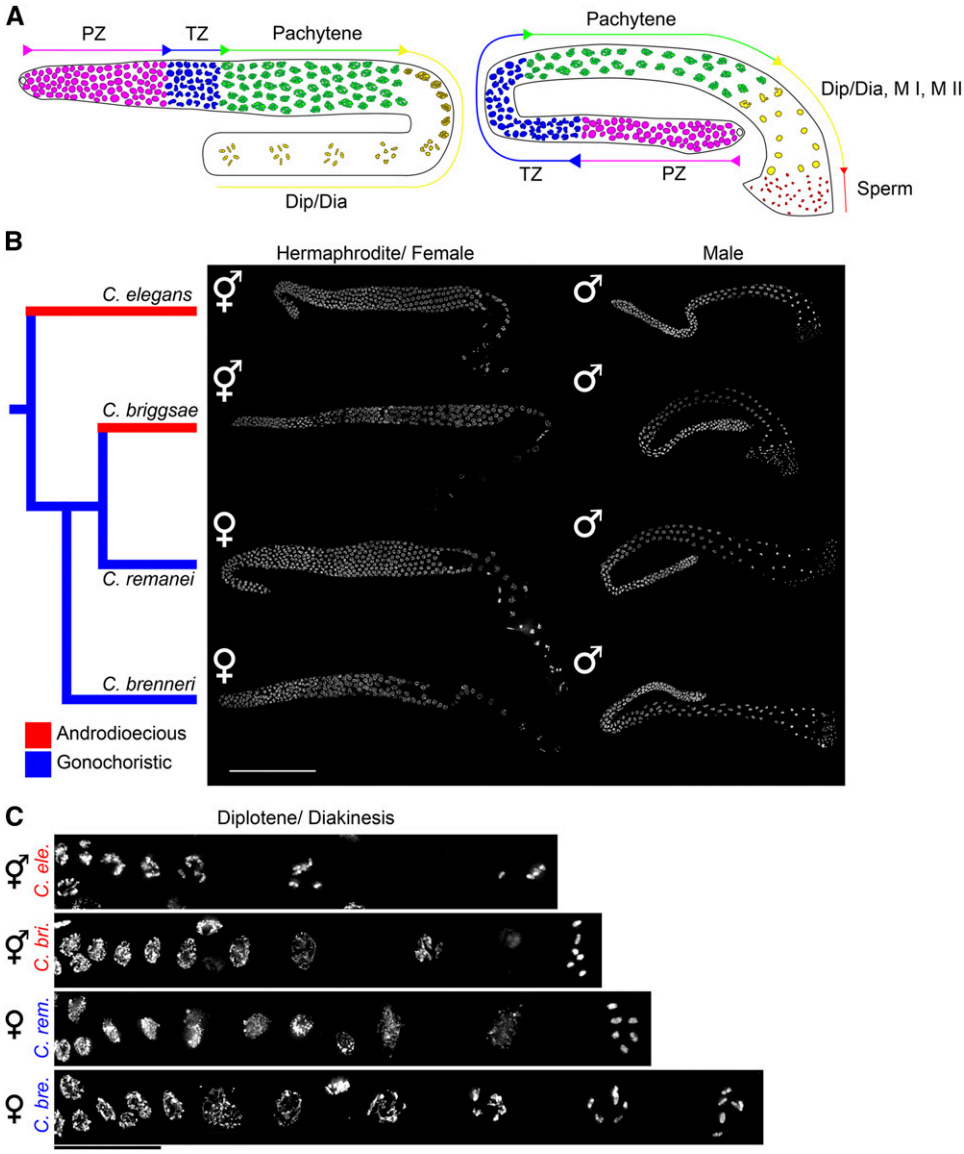

Figure 1 Macro structure and organization of the germ line are conserved among *Caenorhabditis*. (A) Diagrams of the spatiotemporal organization of the female/hermaphrodite and male *Caenorhabditis* germ lines. Dip/Dia, diplotene/diakinesis; MI, meiosis I; MII, meiosis II; PZ, proliferative zone; TZ, transition zone. (B) Full-length DAPI-stained germ lines of *C. elegans*, *C. briggsae*, *C. remanei*, and *C. brenneri* labeled with their phylogenetic relationships (redrawn from Kiontke *et al.* 2011); only one of the two symmetric germ lines is shown for hermaphrodites/females. Bar, 100 μM. (C) Diplotene/diakinesis of female/hermaphrodite germ lines. Images were straightened using Fiji. Bar, 25 μM.

whether MSCI is conserved and influenced by the mode of sexual reproduction, we examined the properties of the X chromosome of males in the four *elegans* group members.

Previous studies revealed that MSCI in *C. elegans* male germ cells manifests in the X chromosome being highly condensed, lacking activating chromatin marks, and being transcriptionally silenced throughout meiotic prophase (Kelly *et al.* 2002; Reuben and Lin 2002; Jaramillo-Lambert and Engebrecht 2010; Checchi and Engebrecht 2011a). To examine the properties of the X chromosome in the different *Caenorhabditis* species, we first stained with antibodies directed against the activating mark histone H3 lysine 4 dimethylation (H3K4me2). In pachytene nuclei, H3K4me2 was observed on all DNA except for one region in all four species, suggesting the DAPI-stained region lacking H3K4me2 was the X (Figure 2A, circle), as previously reported (Kelly *et al.* 2002). A single DAPI-stained body, presumably the X chromosome pair, was also largely lacking H3K4me2 in early pachytene hermaphrodite/female germ cells (Figure S2A).

To confirm that the chromosome lacking H3K4me2 in male germ cells was indeed the X, we examined the loading of SYP-1 or SYP-2, central region components of the SC, which are not present on the X chromosome in pachytene nuclei in *C. elegans* male germ cells (Jaramillo-Lambert and Engebrecht 2010; Checchi *et al.* 2014). To that end, we used antibodies raised against *C. elegans* SYP-1 or SYP-2 peptide sequences with strong sequence identity to the corresponding proteins in the different species (*Materials and Methods*). We found that either SYP-1 or SYP-2 was associated with all chromosomes, except the one that lacked H3K4me2, in pachytene nuclei of all four species (Figure 2B). Thus, the X chromosome in male germ cells of the four *elegans* group species can be identified by the lack of H3K4me2 or SC central components SYP-1/SYP-2. All subsequent experiments used these criteria to identify the X chromosome of males.

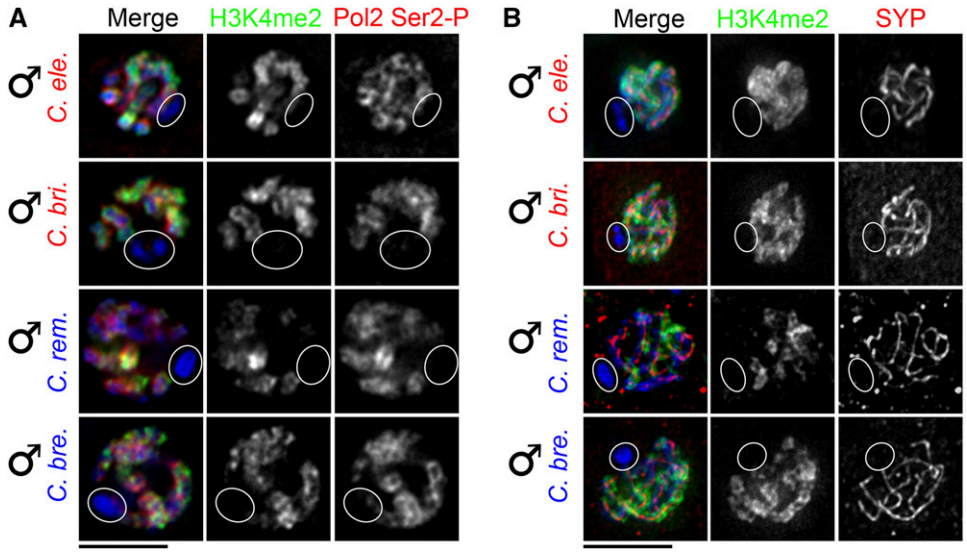

Figure 2 Meiotic sex chromosome inactivation is conserved among *Caenorhabditis*. (A) *C. elegans*, *C. briggsae*, *C. remanei*, and *C. brenneri* pachytene nuclei stained with DAPI (blue), anti-H3K4me2 (green), and anti-Pol2 Ser2-P (red). MSCI was observed in all species, as indicated by the absence of both the promotive chromatin mark H3K4me2 and actively transcribing RNA polymerase (Pol2 Ser2-P) from the X chromosome (circled). (B) Pachytene nuclei stained with DAPI (blue), anti-H3K4me2 (green), and either anti-SYP-2 (red) for *C. elegans* and *C. briggsae* or anti-SYP-1 (red) for *C. remanei* and *C. brenneri*. Identity of the X chromosome was verified by the absence of SC components. Bars, 5 μM.

To determine whether the absence of the activating mark H3K4me2 corresponds to transcriptional silencing, we examined the localization of actively transcribing RNA polymerase II using antibodies directed against phosphorylated serine 2 on the C-terminal domain (Pol2 Ser2-P) (Hsin and Manley 2012). As expected, and in contrast to the autosomes, the chromosome lacking H3K4me2 in all of these species did not stain with Pol2 Ser2-P antibodies, indicating that the X is transcriptionally silenced in male germ cells (Figure 2A). We observed a similar absence of H3K4me2 and Pol2 Ser2-P on the paired X chromosomes in hermaphrodites/females in early and midpachytene in all of the species (Figure S2A). However, Pol2 Ser2-P was detectable on all chromosomes in late pachytene, suggesting that X chromosomes becomes transcriptionally active in *C. briggsae*, *C. remanei*, and *C. brenneri* hermaphrodite/female germ cells in late prophase (Figure S2B), as has been previously reported in *C. elegans* (Reinke *et al.* 2000; Kelly *et al.* 2002). Interestingly, in *C. remanei* and *C. brenneri*, accumulation of Pol2 Ser2-P on the X chromosome pair in late pachytene did not correspond with accumulation of H3K4me2 (Figure S2B). Together, these data indicate that germ cells silence their X chromosome(s) in all of these species, irrespective of sexual mode.

The X chromosome of males is enriched for different repressive marks in different Caenorhabditis species

In *C. elegans*, the X chromosome is highly enriched for the repressive chromatin mark, H3K9me2 (Kelly *et al.* 2002; Reuben and Lin 2002; Bessler *et al.* 2010; Checchi and Engebrecht 2011a). To determine whether the other species also loaded H3K9me2 onto the X chromosome in germ cells, we stained extruded germ lines with antibodies directed against H3K9me2, which we previously used to examine the X chromosome in *C. elegans* germ cells (Checchi and Engebrecht 2011a). We found that similar to *C. elegans*, the X chromosome of *C. remanei* males was enriched for H3K9me2; however, surprisingly, no H3K9me2 staining to a specific region was detected in male germ cells of *C. briggsae* or *C. brenneri*; instead, more diffuse genome-wide staining was observed (Figure 3). Costaining with H3K4me2 and H3K9me2 confirmed the identity of the X chromosome in *C. remanei* germ cells (Figure S3A).

Both the repressive di- and trimethylated forms of H3K9 are enriched on the XY sex body of male germ cells in mice (van der Heijden *et al.* 2007), prompting us to examine the localization of H3K9me3 in *Caenorhabditis* germ lines. To that end, we probed male germ cells of the four *Caenorhabditis* species with antibodies specific for H3K9me3. We found that a single DAPI-stained body in both *C. briggsae* and *C. brenneri* male germ cells was enriched for H3K9me3 (Figure 3). As this chromosome also lacked H3K4me2 (Figure S3B), we conclude that the X chromosome in *C. briggsae* and *C. brenneri* male germ cells is enriched for H3K9me3 instead of H3K9me2 as in *C. elegans* and *C. remanei*. A similar pattern was observed in hermaphrodite/female pachytene germ cells (Figure S3, C and D). Surprisingly, a single focus of H3K9me3 staining was observed in most *C. briggsae* proliferating male germ cell nuclei, while two foci of H3K9me3 enrichment was observed in most hermaphrodite proliferating germ cell nuclei (Figure S3E). These correspond to the single X chromosome in males and two X chromosomes in hermaphrodites and further support our identification of the X chromosome in *C. briggsae*. Furthermore, these results indicate that in *C. briggsae* H3K9me3 enrichment on sex chromosomes is established in proliferating germ cells prior to entry into meiosis. In *C. remanei* germ cell nuclei, H3K9me3 was observed at low levels genome-wide, as in *C. elegans* (Figure 3). Thus, sex chromosomes in closely related *Caenorhabditis* species have distinct germ-line H3K9 methylation patterns.

The regulatory network for deposition of repressive marks on the X chromosome in the C. briggsae germ line is distinct from the pathway in C. elegans

Previous studies in *C. elegans* have shown that the SETDB1 histone methyltransferase, MET-2, is responsible for deposition

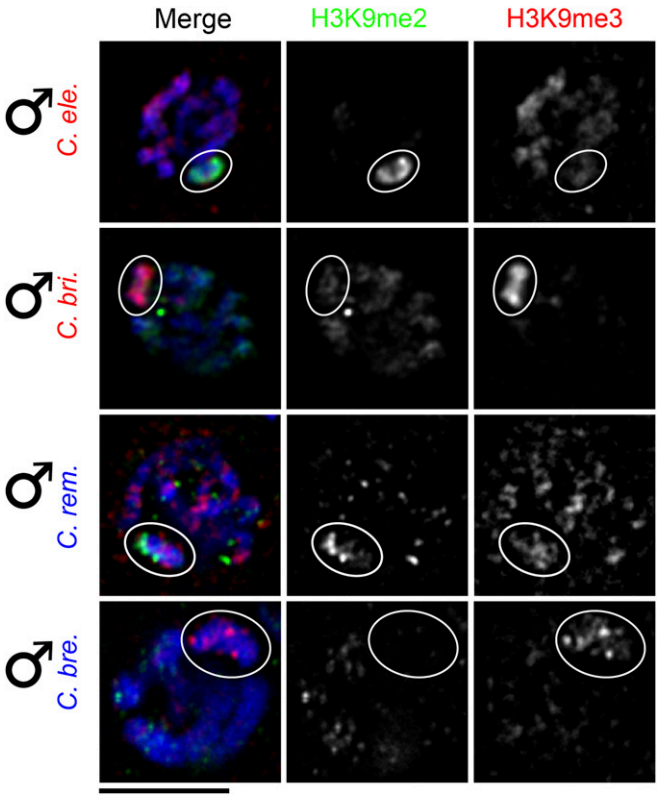

Figure 3 Patterns of the repressive chromatin marks H3K9me2 and H3K9me3 vary among *Caenorhabditis* species at pachytene. *C. elegans*, *C. briggsae*, *C. remanei*, and *C. brenneri* pachytene nuclei stained with DAPI (blue), anti-H3K9me2 (green), and anti-H3K9me3 (red). In *C. elegans* and *C. remanei*, the X chromosome (circled) was enriched with H3K9me2, while in *C. briggsae* and *C. brenneri*, the X chromosome was enriched with H3K9me3. Bar, 5 μM.

of H3K9me2 on the X chromosome(s) in germ cells of *C. elegans* males and hermaphrodites (Bessler *et al.* 2010). Interestingly, mutation of MET-2 abrogated H3K9me2 deposition but did not affect H3K9me3 accumulation, while inactivation of the Polycomb Repressive Complex 2-related histone methyltransferase MES-2 (Holdeman *et al.* 1998) resulted in depletion of H3K9me3 but not H3K9me2, suggesting that these marks are acquired independently in the *C. elegans* germ line (Bessler *et al.* 2010). To examine the gene network responsible for deposition of H3K9me2 and H3K9me3 in the germ line in a species that accumulates H3K9me3 on sex chromosomes, we depleted histone methyltransferases in *C. briggsae* strains expressing *C. elegans* SID-2 from an integrated chromosomal array, which makes them susceptible to RNAi by feeding (Nuez and Felix 2012). Additionally, these strains allowed us to examine the chromatin state of a multicopy array, which in *C. elegans* is enriched for H3K9me3 in germ cells when the array carries a somatically expressed gene (Bessler *et al.* 2010). Indeed, these strains had two regions of enhanced H3K9me3 staining throughout prophase (Figure 4A, circles), suggesting that the array is also enriched for H3K9me3 in *C. briggsae* germ cells.

We first investigated the consequence of inactivating the *Cbr*-MET-2 ortholog by examining the germ lines of the progeny of worms continuously fed *Cbr-met-2* double-strand RNA (dsRNA). In contrast to *C. elegans met-2* mutants, germ-line nuclei from the proliferative zone to early pachytene in *Cbr-met-2*(RNAi) worms were largely devoid of both H3K9me2 and H3K9me3 (Figure 4A); however, by midpachytene a single region of H3K9me3 was observed, which based on further observation, most likely corresponded to the integrated array (see Figure 6). Thus, *Cbr*-MET-2 is important for the acquisition of both H3K9me2 and H3K9me3 in germ cells; however, additional methyltransferase(s) contributes to H3K9me3 deposition on the array beginning in midpachytene. These results suggest that unlike *C. elegans*, the acquisition of H3K9me2 and H3K9me3 are interdependent in *C. briggsae* germ cells. Alternatively, *Cbr*-MET-2 may catalyze the addition of both H3K9 di- and trimethylation.

To distinguish between these possibilities, we depleted the methyltransferases *Cbr*-MES-2 and *Cbr*-SET-25, which mediate the conversion of H3K9me2 to H3K9me3 in *C. elegans* germ cells and embryos, respectively (Bessler *et al.* 2010; Towbin *et al.* 2012). Furthermore, inactivation of *Cel-set-25* by RNAi revealed elevated levels of germ-line H3K9me2, indicating that SET-25 also functions in the *C. elegans* germ line to convert H3K9me2 to H3K9me3 (Figure S4A). Following depletion of either *Cbr*-MES-2 or *Cbr*-SET-25, we observed elevated H3K9me2 in the TZ and early pachytene germ-line nuclei, including the H3K9me3-associated regions, which represent the X and array (Figure 4A). However, by midpachytene, no differences were observed. Furthermore, simultaneous depletion of *Cbr-mes-2* and *Cbr-set-25* did not result in further accumulation of H3K9me2 (Figure S4C). Taken together, these results suggest that either depletion was incomplete and/or that additional methyltransferases contributed to conversion of H3K9me2 to H3K9me3. Nonetheless, these results support the hypothesis that both MES-2 and SET-25 contribute to conversion of H3K9me2 to H3K9me3 and that H3K9me2 and H3K9me3 acquisition are interdependent in the *C. briggsae* germ line.

C. briggsae met-2 mutants are defective for germ-line H3K9me2/me3 acquisition and MSCI

Depletion of *Cbr-met-2* resulted in a different phenotype than that observed in *Cel-met-2* mutants (Bessler *et al.* 2010), suggesting that MET-2 function and/or regulation has diverged between these species. Alternatively, *Cbr-met-2*(RNAi) may have had off-target effects, resulting in removal of both H3K9me2 and H3K9me3. To distinguish between these possibilities, we generated deletion mutations of *Cbr-met-2* using clustered regularly interspaced short palindromic repeats (CRISPR)-Cas9 with dual sgRNAs as described for *C. elegans* (Chen *et al.* 2014) (Figure 5A). We isolated two independent deletions: *Cbr-met-2(xoe1)* and *Cbr-met-2(xoe2)*. *Cbr-met-2(xoe1)* is missing 1682 bp with an insertion of 15 bp; the deletion removes part of exon 7, all of exon 8, and most of exon 9, covering sequence coding for the DNA binding

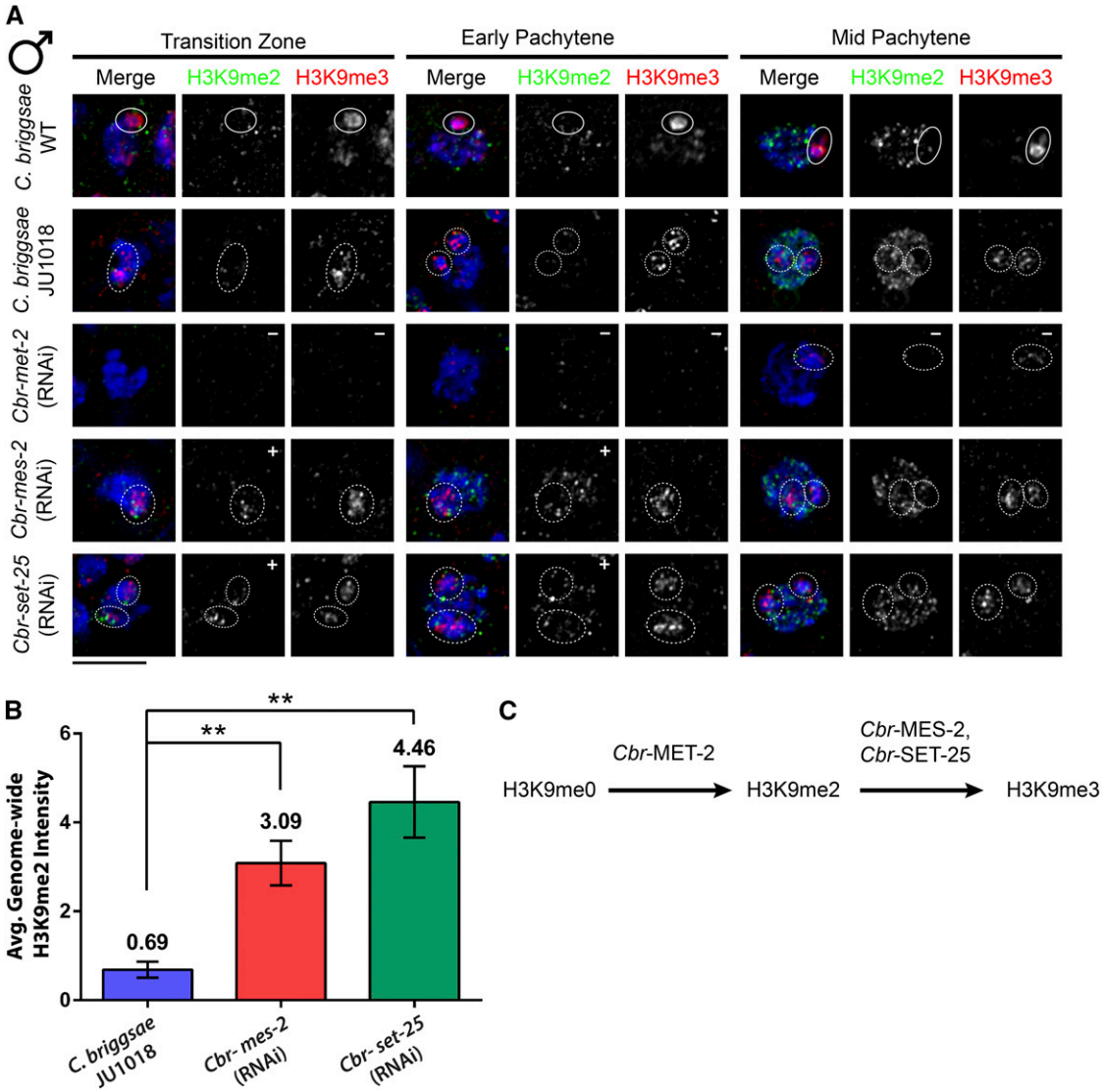

Figure 4 The *C. briggsae* male X chromosome is methylated to H3K9me3 in a stepwise fashion. (A) *C. briggsae* nuclei stained with DAPI (blue), anti-H3K9me2 (green), and anti-H3K9me3 (red). Genome-wide H3K9me2 was observed at midpachytene, while the single X chromosome (circled) was enriched for H3K9me3 at all stages. In the RNAi-sensitive feeding strain, JU1018, an additional H3K9me3-enriched area was present and is presumed to be the integrated transgene array. *Cbr-met-2* RNAi-treated worms have severely reduced levels of H3K9me2 and H3K9me3 at all stages (−); however, one region of H3K9me3 was observed in pachytene, which is most likely the array. Both *Cbr-mes-2* and *Cbr-set-25* RNAi-treated worms had ectopic H3K9me2 at transition zone and early pachytene (+), while H3K9me3 appeared unchanged. Dotted circles indicate the X chromosome/integrated transgene array. Bars, 5 μM. (B) Graph comparing the average genome-wide H3K9me2 levels in early pachytene nuclei. ** $P < 0.001$; $n > 20$ for each genotype. (C) Model for H3K9me3 acquisition in the *C. briggsae* germ line.

domain (DBD), pre-SET domain, and approximately half of the essential SET domain (Xiao *et al.* 2003) (Figure 5, B and C). Additionally, the deletion results in the introduction of an early stop codon, which is predicted to produce a 643-aa product [MET-2(ΔC)] compared to the 1269-aa WT protein. Together, the large deletion and introduction of an early stop codon strongly suggest *met-2(xoe1)* is a null mutation. On the other hand, *Cbr-met-2(xoe2)* deletes 1026 bp with a 5-bp insertion (Figure 5, B and C). The mutation is predicted to generate an in-frame deletion that removes the DBD and most of the pre-SET domain, which is important for structural stability, but keeps the SET domain intact [MET-2-(ΔDBD/pre-SET)]. Thus, this mutation should disrupt regulated histone methylation, but may not be a null mutation.

To examine the phenotype *Cbr-met-2(xoe1)* and *Cbr-met-2(xoe2)*, we monitored H3K9me2 and H3K9me3 in the corresponding germ lines. Consistent with our analysis of *Cbr-met-2*(RNAi), we observed neither H3K9me2 nor H3K9me3 in pachytene germ cells of *Cbr-met-2(xoe1)* (Figure 5D). In *Cbr-met-2(xoe2)*, instead of a single DAPI-stained body enriched for H3K9me3, we observed both H3K9me2 and H3K9me3 in punctate structures throughout the genome, suggesting that this mutant protein improperly targets

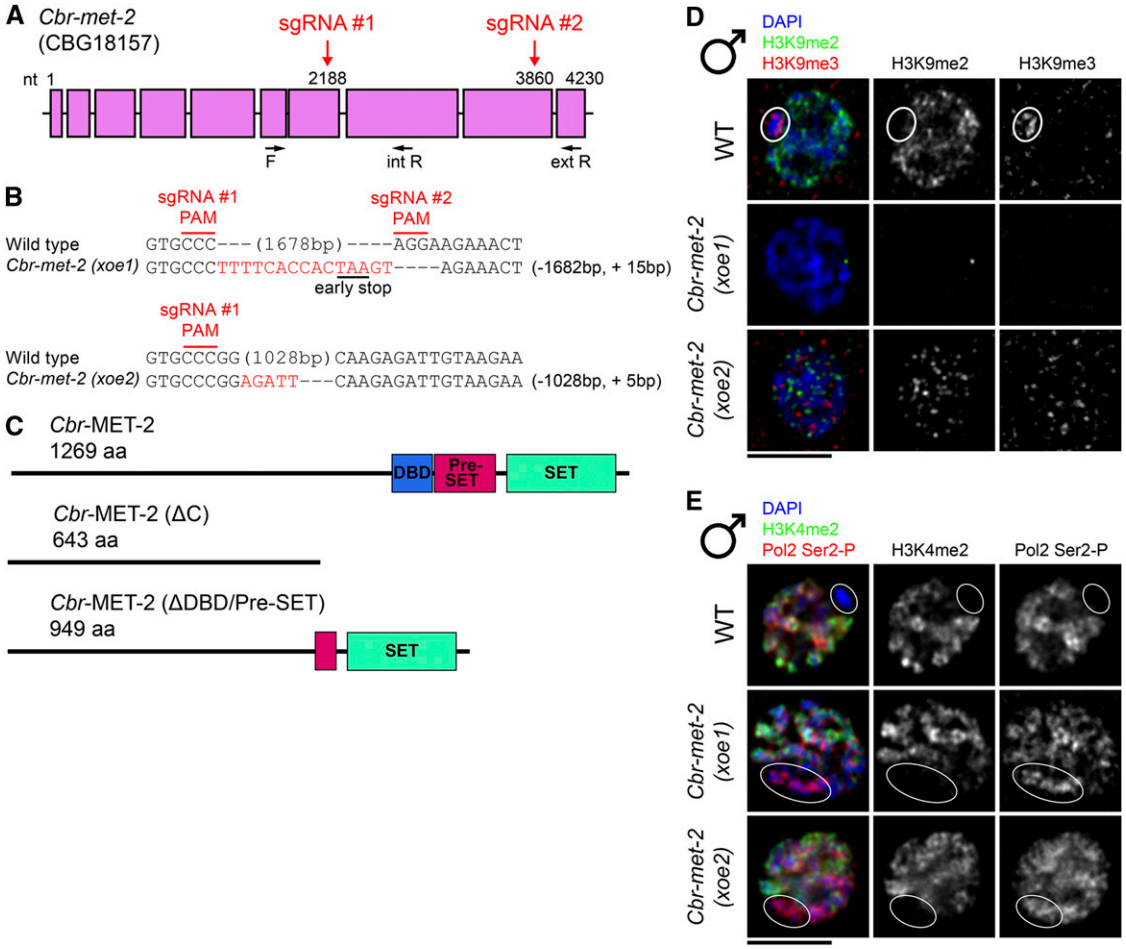

Figure 5 C. *briggsae met-2* mutants are defective for MSCI. (A) Diagram of *Cbr-met-2* (CBG18157) locus; cut sites of sgRNAs (red arrows) and PCR primers used for screening (black arrows) are indicated. (B) Sequence alignments of WT and mutant alleles. Numbers of base pairs deleted/inserted are indicated on the right. *Cbr-met-2(xoe1)* contains an indel that introduces an early stop codon. *Cbr-met-2(xoe2)* contains an indel that introduces two missense amino acid codons, but maintains the reading frame of the remaining sequence. (C) Predicted protein products of WT *Cbr*-MET-2 and mutant alleles. The *Cbr*-MET-2 protein contains three recognized protein domains: methyl-CpG DBD, zinc binding pre-SET, and SET. The indel in *Cbr-met-2(xoe1)* introduces an early stop codon resulting in loss of DBD, pre-SET, and SET domains [*Cbr*-MET-2 (ΔC)]. The indel in *Cbr-met-2(xoe2)* removes DBD and a large portion of pre-SET, but leaves the SET domain intact [*Cbr*-MET-2 (ΔDBD/pre-SET)]. (D) WT, *Cbr-met-2(xoe1)*, and *Cbr-met-2(xoe2)* pachytene nuclei stained with DAPI (blue), anti-H3K9me2 (green), and anti-H3K9me3 (red). No H3K9me2 or H3K9me3 was observed in *Cbr-met-2(xoe1)*, while punctate H3K9me2 and H3K9me3 were observed in *Cbr-met-2(xoe2)*. (E) WT, *Cbr-met-2(xoe1)*, and *Cbr-met-2(xoe2)* pachytene nuclei stained with DAPI (blue), anti-H3K4me2 (green), and anti-Pol2 Ser2-P (red). Ectopic transcription was observed on the X chromosome in both *Cbr-met-2(xoe1)* and *Cbr-met-2(xoe2)* mutants.

H3K9me2/me3 (Figure 5D). Together, these results support the hypothesis that *Cbr*-MET-2 is responsible for the deposition of H3K9me2 genome-wide, and its inactivation blocks the conversion of H3K9me2 to H3K9me3 on the X chromosome in the *C. briggsae* germ line.

To determine the functional consequence of removal of germ-line H3K9me2 and H3K9me3, we examined *Cbr-met-2(xoe1)* and *Cbr-met-2 (xoe2)* mutant germ lines for accumulation of the activating mark H3K4me2 and Pol2 Ser2-P. While we observed no accumulation of H3K4me2 on the X chromosome, Pol2 Ser2-P was detected, suggesting a failure in MSCI. We also examined progeny viability and brood size and, although *Cbr-met-2(xoe1)* mutants had slightly higher progeny inviability and smaller brood sizes, these were not significantly different than WT [progeny inviability: 2.79 ± 0.76% WT *vs.* 5.43 ± 2.36% *met-2(xoe1)*, $P = 0.30$ Student's *t*-test; brood size: 152 ± 4 WT *vs.* 140 ± 5 *met-2(xoe1)*, $P = 0.09$ Student's *t*-test]. *C. elegans met-2* mutants display a weak germ-line mortality (Mrt) phenotype after 18–28 generations (Ahmed and Hodgkin 2000; Andersen and Horvitz 2007). To determine whether *Cbr-met-2(xoe1)* also had a Mrt phenotype, we propagated *C. briggsae* WT and *met-2(xoe1)* mutants for 30 generations and saw no differences in fertility, suggesting that *C. briggsae* MET-2 is not critical for germ-line immortality. Taken together, we discovered that in contrast to *C. elegans*, *C. briggsae* germ cells acquire the repressive marks H3K9me2 and H3K9me3 sequentially; however, in both species, sex chromosome enrichment of H3K9 methylation is dependent on MET-2 and removal of these marks from the X chromosome results in disruption of MSCI.

MET-2-dependent H3K9me3 is redistributed in the presence of asynapsed chromosomes in the C. briggsae male germ line

In addition to hemizygous sex chromosomes, asynapsed regions of homologous chromosomes are also epigenetically marked in the MSUC process. MSCI and MSUC have been proposed to be related, as both result in deposition of repressive chromatin on unpaired chromosomes (Turner 2007). In *C. elegans*, H3K9me2 decorates both the X and asynapsed autosomes (Bean *et al.* 2004; Maine *et al.* 2005; Checchi and Engebrecht 2011a; Lamelza and Bhalla 2012). To determine whether H3K9me3 decorated asynapsed chromosomes as it does on the X in *C. briggsae* germ cells, we induced asynapsis by growing *C. briggsae* containing *C. elegans* SID-2 on *Escherichia coli* expressing dsRNAs directed against the HIM/ZIM family of zinc finger proteins. These proteins recognize a different set(s) of chromosome-specific pairing centers (PCs) and their inactivation results in asynapsis of the corresponding chromosome(s) (Phillips *et al.* 2005; Phillips and Dernburg 2006). For this analysis, we constructed feeding vectors for *Cbr-zim-1* (ZIM-1 binds chromosomes II and III PCs) and *Cbr-zim-2* (ZIM-2 binds chromosome V PCs) based on the analysis of the corresponding genes in *C. elegans* (Phillips and Dernburg 2006). We confirmed that RNAi treatment resulted in knockdown by examining the number of DAPI-stained bodies at diakinesis in hermaphrodites [WT: 6 ± 0 *vs.* *Cbr-zim-1*(RNAi) 7.6 ± 0.1, $P < 0.0001$ Student's *t*-test *vs.* *Cbr-zim-2*(RNAi): 6.3 ± 0.06, $P < 0.0001$ Student's *t*-test] and stained the corresponding male germ lines for H3K9me2 and H3K9me3.

In pachytene nuclei, the *C. briggsae* RNAi feeding-sensitive strain had two genomic regions enriched for H3K9me3: the X chromosome and the chromosome harboring the integrated array (Figure 6A, arrows). If a single pair of asynapsed chromosomes were enriched for H3K9me3, we would predict three or four regions of H3K9me3 enrichment, depending on whether or not the asynapsed chromosomes harbored the array, which is already enriched for H3K9me3. We found that worms depleted for *Cbr*-ZIM-2, showed three prominent regions of H3K9me3 (Figure 6A, arrows), suggesting that the array integrated onto chromosome V, but confounding whether or not H3K9me3 is enriched on asynapsed chromosomes. In light of this, we depleted ZIM-1, as we predicted that there would be six regions (X, array, and asynapsed IIs and IIIs) of H3K9me3 enrichment if H3K9me3 decorated asynapsed chromosomes or two regions of enrichment (X and array) if it did not. Contrary to these predictions, we observed that H3K9me3 was dispersed throughout the genome in the absence of *Cbr*-ZIM-1 (Figure 6A). In support of change in distribution, there was no statistical difference between genome-wide H3K9me3 levels in the presence and absence of *Cbr*-ZIM-1 (Figure 6B). Thus, chromosome asynapsis leads to redistribution of limiting H3K9me3, suggesting that in *C. briggsae*, both MSCI and MSUC are mediated by H3K9me3.

To examine the effect of asynapsis on silencing, we monitored the transcriptional state of the chromatin using an antibody raised against the serine 5 phosphoepitope on the C-terminal domain of polymerase II (Pol2 Ser5-P) (Hsin and Manley 2012) in *Cbr-zim-1*(RNAi) germ lines. Consistent with some H3K9me3 being redistributed from the X to asynapsed chromosomes, we observed very low levels of Pol2 Ser5-P on the X (Figure 6C, white dashed circles). However, asynapsed chromosomes, as marked by the absence of SYP-2, had similar levels of Pol2 Ser5-P as synapsed chromosomes (Figure 6D). Thus, this analysis suggests that the pool of H3K9me3 is limiting and when multiple asynapsed chromosomes are present, meiotic silencing is not efficient.

To determine whether MET-2 is responsible for the H3K9me3 that is dispersed throughout the genome upon induction of asynapsis, we generated *C. briggsae met-2(xoe1)*; *Cel-sid-2*$^{+}$ worms and grew them on *E. coli* expressing dsRNA against the *him/zim* genes. Consistent with our previous analysis (Figure 5), deletion of MET-2 significantly reduced levels of both H3K9me2 and H3K9me3. However, in midpachytene H3K9me3 was observed on the integrated array as verified by *Cbr-zim-2* inactivation, where two domains of H3K9me3 were observed (Figure 6E). When multiple asynapsed chromosomes were present following depletion of *Cbr*-ZIM-1 in *Cbr-met-2(xoe1)*, no enrichment of H3K9me3 was observed, and in fact, there were overall lower levels of H3K9me3 (Figure 6B). Together, these results indicate that *Cbr*-MET-2 contributes to the generation of H3K9me3, which decorates both the single X chromosome and asynapsed autosomes; however, this mark is limiting in the male germ line.

Sex-specific differences in meiotic silencing

In mice, chromosome asynapsis triggers different extents of silencing in male and female germ cells, presumably due to the presence of the constitutively unpaired sex chromosomes in males and limiting silencing machinery (reviewed in Turner 2015). To determine whether chromosome asynapsis resulted in differences with respect to silencing in *C. briggsae* males and hermaphrodites, we examined H3K9me2 and H3K9me3 deposition in germ lines of hermaphrodites treated with RNAi against the *him/zim* family members (Figure 7A). In pachytene nuclei, we observed two regions of H3K9me3 deposition, which were the paired Xs (dashed circle) and the array on the paired chromosome Vs (Figure 7A, yellow arrow); we used size, morphology, and nuclear position to distinguish the X from the chromosome harboring the array. At diakinesis, the chromosome V bivalent was observed with discrete regions of H3K9me3 marking the array (yellow arrow). Inactivation of either *Cbr-him-8*, which results in X chromosome asynapsis (Phillips *et al.* 2005), or *Cbr-zim-2*, which results in chromosome V asynapsis (Phillips and Dernburg 2006), resulted in three H3K9me3-enriched regions [*him-8*-(RNAi): two unpaired Xs and paired Vs; *zim-2*(RNAi): two unpaired Vs and paired Xs] (Figure 7A, dashed circle and yellow arrows). The bivalent (*him-8*) or univalents (*zim-2*,

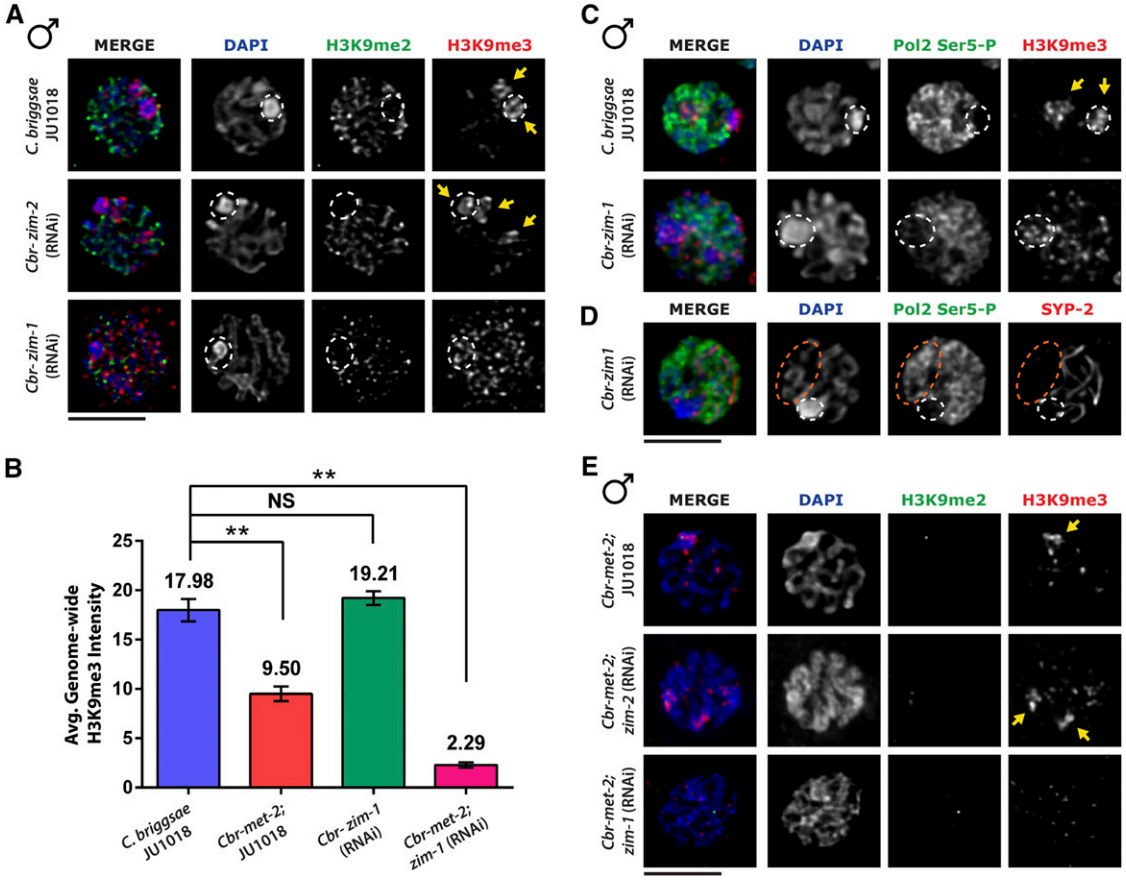

Figure 6 Meiotic silencing of unpaired chromosomes in *C. briggsae* males. (A and E) Pachytene nuclei stained with DAPI (blue), anti-H3K9me2 (green), and anti-H3K9me3 (red) from male *C. briggsae* of the given genotypes; *Cbr-met-2(xoe1)* was used for this analysis. Yellow arrows point to chromosomes enriched for H3K9me3. White dashed circles signify the presumed X chromosome based on morphology, nuclear positioning, and enrichment for H3K9me3. Bars, 5 μM. (B) Graph comparing the average genome-wide H3K9me3 levels. The significance of the difference is depicted as follows: NS, nonsignificant, ** $P < 0.001$; $n > 20$ for each genotype. (C) Pachytene nuclei stained with DAPI (blue), anti-Pol2 Ser5 (green), and anti-H3K9me3 (red) from male *C. briggsae* of the given genotypes. Yellow arrows point to chromosomes enriched for H3K9me3. White dashed circles signify the presumed X chromosome. Bars, 5 μM. (D) Pachytene nuclei stained with DAPI (blue), anti-Pol2 Ser5 (green), and anti-SYP-2 (red) from *Cbr-zim-1*(RNAi) males. Orange dashed circle denotes region of asynapsed chromosomes. White dashed circles mark the presumed X chromosome.

white arrows) carrying the array were clearly visible at diakinesis. In *Cbr-zim-1* (RNAi), genome-wide H3K9me3 was observed but two regions had more intense staining, which most likely represented the paired Xs and Vs. Interestingly, and in contrast to males, overall higher levels of H3K9me3 were observed in *zim-1* (RNAi) germ cells, suggesting that chromosome asynapsis induces higher levels of H3K9me3 in female compared to male germ cells (Figure 7C).

We next examined the role of *Cbr*-MET-2 in H3K9me3 deposition in response to chromosome asynapsis in hermaphrodites. In *Cbr-met-2(xoe1)*, no H3K9me3 was detected on the Xs but H3K9me3 was still observed on the array at both pachytene and diakinesis (Figure 7B, yellow arrows), as reflected by the reduction, but not elimination, in overall H3K9me3 levels compared to WT ($P < 0.001$ Student's *t*-test; Figure 7C). Consistent with this, HIM-8 depletion, resulted in a single region of H3K9me3, which presumably represents the array on the paired chromosome Vs, while *zim-2* depletion resulted in two regions of H3K9me3, which presumably represents the array on the unpaired chromosome Vs (Figure 7B). Further, multiple asynapsed chromosomes in *Cbr-met-2(xoe1)*; *zim-1* (RNAi) resulted in a small reduction in genome-wide H3K9me3 levels ($P < 0.05$ Student's *t*-test), which was significantly smaller than the reduction observed in male germ cells (hermaphrodites: 1.2-fold *vs.* males: 8.4-fold reduction; compare Figure 7, B and C to Figure 6, B and C). These results suggest that additional histone methyltransferases play a more prominent role in H3K9me3 deposition in response to chromosome asynapsis in the hermaphrodite germ line compared to the male germ line.

To determine the transcriptional status of asynapsed chromosomes in hermaphrodites, we stained germ lines from *Cbr-zim-1* (RNAi) worms with SYP-2, to monitor synapsis, and Pol2 Ser5-P, to monitor transcription (Figure 7D). Unlike the situation in males where asynapsed chromosomes were labeled with Pol2 Ser5-P (Figure 7D), a significant proportion of asynapsed chromosomes in hermaphrodite germ cells failed to load Pol2 Ser5-P (33.7% of pachytene nuclei; Figure

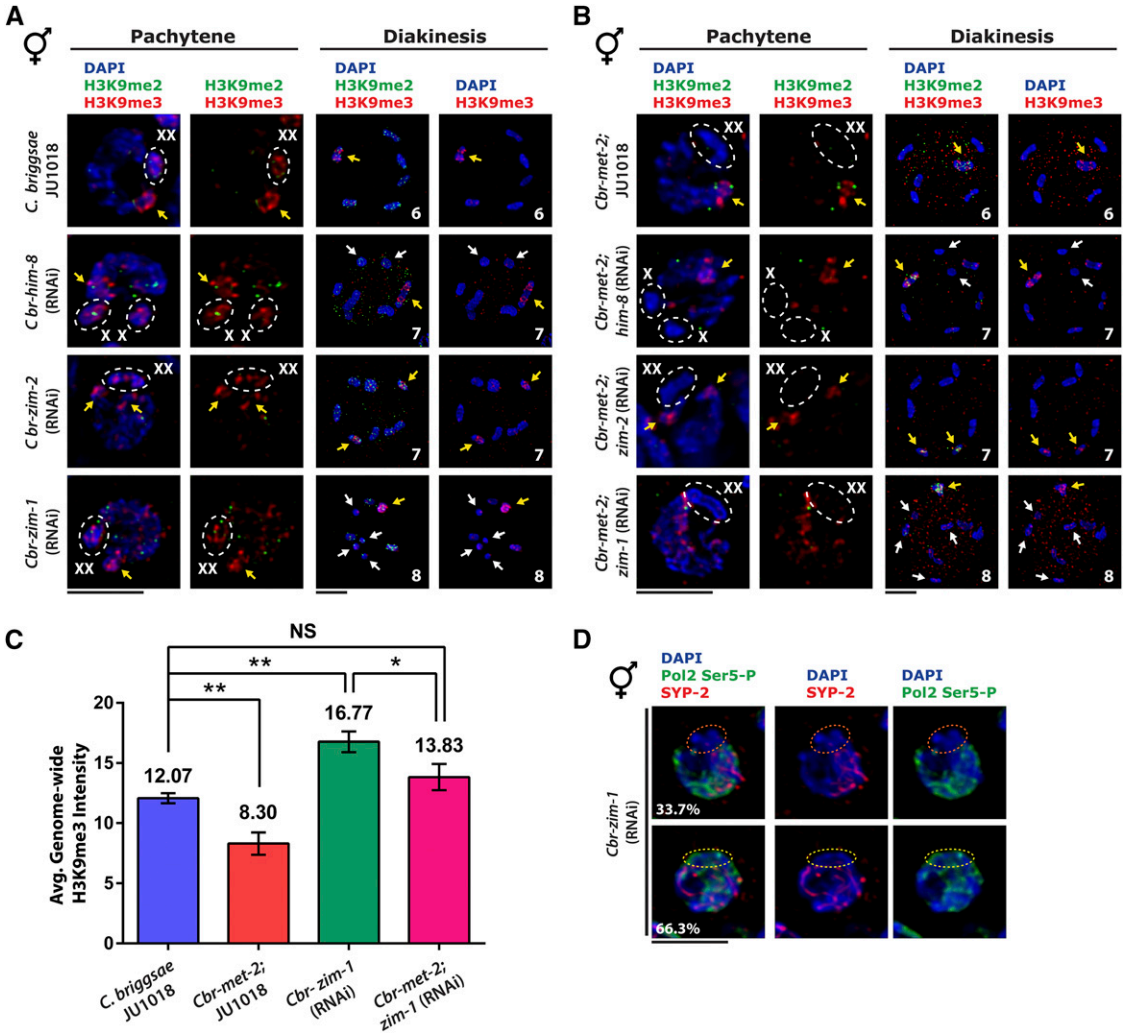

Figure 7 Meiotic silencing of unpaired chromosomes in *C. briggsae* hermaphrodites. (A and B) Pachytene nuclei stained with DAPI (blue), anti-H3K9me2 (green), and anti-H3K9me3 (red) from hermaphrodite *C. briggsae* of the given genotypes; *Cbr-met-2(xoe1)* was used for this analysis. White dashed circles signify the presumed X chromosome based on morphology, nuclear positioning, and enrichment for H3K9me3. Yellow arrows mark the presumed chromosome V with integrated array. White arrows indicate univalents. Number of DAPI bodies observed at diakinesis is indicated. Bars, 5 μM. (C) Graph comparing the average genome-wide H3K9me3 levels. The significance of the difference is depicted as follows: NS, nonsignificant; * $P < 0.05$, ** $P < 0.001$; $n > 20$ for each genotype. (D) Pachytene nuclei stained with DAPI (blue), anti-Pol2 Ser5 (green), and anti-SYP-2 (red) from *Cbr-zim-1*(RNAi) hermaphrodites. Orange dashed circle denotes asynapsed chromosomes that lack Pol2 Ser5-P; yellow dashed circle signifies asynapsed chromosomes that contain Pol2 Ser5-P. Bars, 5 μM.

7B). These results indicate that asynapsed chromosomes have an increased likelihood of being silenced in hermaphrodite *vs.* male germ cells. Thus, in hermaphrodites, the absence of a constitutively unpaired sex chromosome and MET-2-independent deposition of H3K9me3 provide additional H3K9me3 for decoration of asynapsed chromosomes leading to more efficient silencing.

The absence of Cbr-MET-2 results in germ-line checkpoint activation

Errors in chromosome synapsis induce checkpoints, which often lead to elimination of defective germ cells by apoptosis (Bhalla and Dernburg 2005; Morelli and Cohen 2005; Burgoyne *et al.* 2009). We previously found that the single X chromosome of *C. elegans* males is not recognized as partnerless by meiotic checkpoints (Jaramillo-Lambert and Engebrecht 2010), and MET-2 plays a critical role in this process (Checchi and Engebrecht 2011a). To determine whether repressive chromatin deposition on the *C. briggsae* X chromosome of males was important for blocking recognition by checkpoints, we examined levels of phosphorylated CHK-1 in *C. briggsae* germ lines by antibody staining. In response to unrepaired recombination intermediates, ATR (ATL-1 in *Caenorhabditis*) phosphorylates CHK-1 on serine 345 (S350 in *C. briggsae* CHK-1) and activates a signaling cascade that facilitates repair and can induce apoptosis (Liu *et al.* 2000; Jaramillo-Lambert and Engebrecht 2010). *C. briggsae* germ lines have very few phospho-CHK-1 foci, which were abrogated upon CHK-1 depletion by RNAi (2.33 ± 0.21 *vs.* 0.55 ± 0.11; $P < 0.001$ Student's *t*-test). Significantly more

phospho-CHK-1 foci were observed upon induction of chromosome asynapsis by inactivation of *Cbr-zim-1* (5.38 ± 0.39 *vs.* 2.33 ± 0.21 in WT; 2.3-fold; $P < 0.001$ Student's *t*-test) (Figure 8A), which in *C. elegans*, results in activation of the recombination checkpoint (Bhalla and Dernburg 2005), suggesting that chromosome asynapsis also induces checkpoint activation in *C. briggsae* germ cells. *Cbr-met-2(xoe1)* mutants had the highest number of phospho-CHK-1 foci in pachytene germ cells, suggesting that meiotic checkpoints are activated in the absence of MET-2 (9.03 ± 0.54 *vs.* 2.33 ± 0.21 in WT; 3.9-fold; $P < 0.001$ Student's *t*-test) (Figure 8A).

We also examined phospho-CHK-1 in *C. briggsae* hermaphrodite germ cells. As with males, few phospho-CHK-1 foci were detected in WT germ cells, and foci were elevated in *zim-1*(RNAi) germ lines to higher levels than observed in males [WT: 4.47 ± 0.41 *vs.* *zim-1*(RNAi): 14.19 ± 0.61; 3.2-fold; $P < 0.001$ Student's *t*-test]. This difference may reflect differences in checkpoint activation and/or RNAi efficiency in the sexes. On the other hand, a much smaller increase in phospho-CHK-1 foci was observed in *met-2(xoe1)* mutant hermaphrodite (6.79 ± 0.47 *vs.* 4.47 ± 0.41 in WT; 1.5-fold; $P < 0.001$ Student's *t*-test) compared to male germ cells (1.5 *vs.* 3.9-fold increase over WT levels; $P < 0.01$ Student's *t*-test) (Figure 8B), suggesting that *Cbr*-MET-2 is important for shielding the single X chromosome of males from checkpoint machinery. The small increase in phospho-CHK-1 foci in *Cbr-met-2(xoe1)* female germ cells is consistent with slightly elevated levels of apoptosis observed in *Cel-met-2* hermaphrodite germ lines (Mlynarczyk-Evans *et al.* 2013). Together, these results suggest that similar to *Cel*-MET-2, *Cbr*-MET-2 is required for preventing the X chromosome of males from being recognized as partnerless and inducing checkpoint activation.

X chromosomes replicate late in S phase in both C. elegans and C. briggsae germ cells independent of H3K9me2 or H3K9me3 deposition

In addition to transcriptional silencing, the X chromosome(s) of *C. elegans* male and female germ cells replicates late in S phase (Jaramillo-Lambert *et al.* 2007). To determine whether this property is conserved, we monitored incorporation of 5-Ethynyl-2′-deoxyuridine (EdU), a thymidine analog, using the feeding method of Schedl and colleagues (Fox *et al.* 2011) in *C. briggsae* males. Similar to what was observed in *C. elegans* following labeling (Jaramillo-Lambert *et al.* 2007; Mlynarczyk-Evans *et al.* 2013), most germ cell nuclei fall into one of two categories: One, those nuclei that were in early-to-mid S phase at the time of labeling and for which the bulk of the DNA incorporated EdU, except for one DAPI-stained body. Two, those in late S phase at the time of labeling where a single-labeled DAPI-stained body was detected (Figure 9). In both cases, the differentially labeled DAPI-stained body was the X chromosome, as it also lacked H3K4me2. A similar pattern was observed in hermaphrodites (Figure S5A). Thus, late replication is a conserved feature of X chromosomes in both *C. elegans* and *C. briggsae* germ cells.

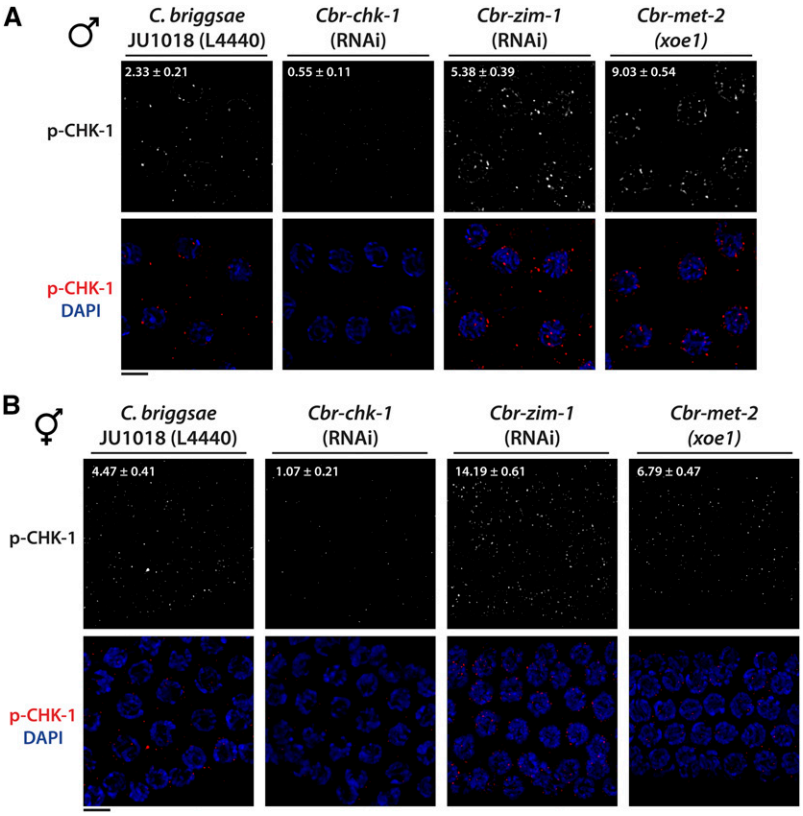

Figure 8 Phospho-CHK-1 staining in *C. briggsae*. (A and B) Pachytene nuclei stained with DAPI (blue) and anti-p-Chk1 (Ser345) (red) from male and hermaphrodite *C. briggsae* of the given genotypes. Each genotype within each sex is significantly different from each other (Student's *t*-test, $P < 0.001$; $n > 20$ for each genotype). The mean and SEM for each genotype is labeled in white. Bars, 5 μM.

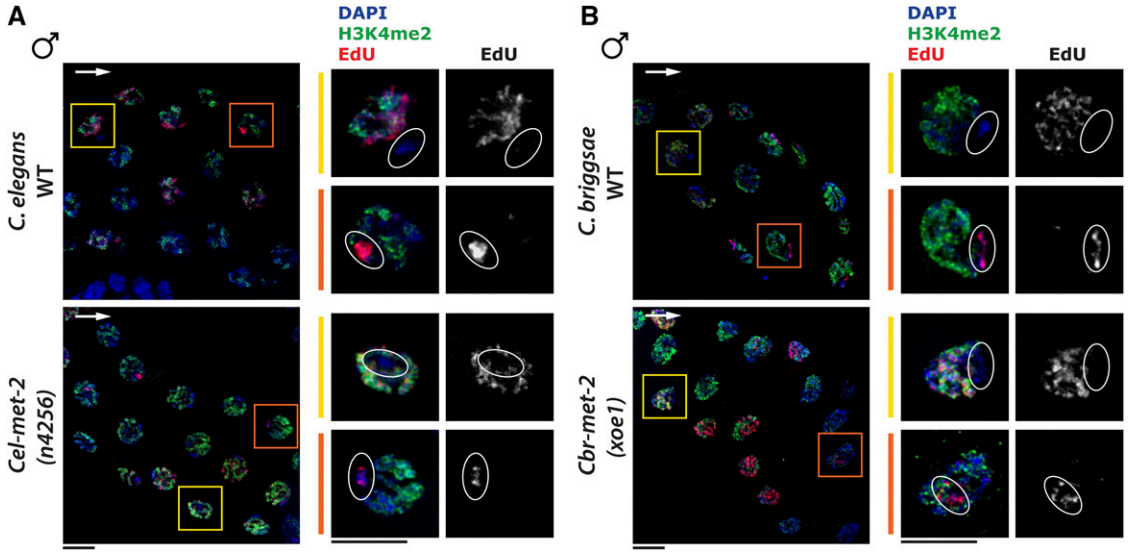

Figure 9 Late replication of the X chromosome in germ-line S phases is not dependent on MET-2 in either *C. elegans* or *C. briggsae* males. (A and B) *C. elegans* and *C. briggsae* EdU (red) labeled pachytene nuclei stained with DAPI (blue) and anti-H3K4me2 (green). White arrow indicates direction of meiotic progression. X chromosomes (identified by the absence of H3K4me2) are circled. Examples of nuclei early in S phase and late in S phase are marked by yellow and orange boxes/lines, respectively. Bars, 5 μM.

Heterochromatic and H3K9me3-enriched regions of the genome tend to replicate late in S phase (Mendez 2009). To determine whether late replication of sex chromosomes was a consequence of enrichment of H3K9me2 and/or H3K9me3, we examined germ cell replication in the absence of MET-2 in both *C. elegans* and *C. briggsae*. While inactivation of *met-2* abrogated the accumulation of H3K9me2 and both H3K9me2 and H3K9me3 in *C. elegans* and *C. briggsae*, respectively, there was no obvious effect on the replication program in either male or female germ cells as monitored by EdU labeling (Figure 9 and Figure S5A). Thus, the replication program is not influenced by the presence of the repressive marks H3K9me2 and/or H3K9me3. We also noted that in the *C. briggsae* RNAi feeding strain, a second region of the genome was also late replicating, which we presume to be the integrated array (Figure S5B). Thus, while accumulation of H3K9me2/me3 does not grossly influence the replication timing of the X chromosome, these results suggest that the integrated array and sex chromosomes have a property in common that dictates late replication.

Diverse patterns of X chromosome H3K9 methylation in male germ cells are observed across the Caenorhabditis phylogeny

The unexpected finding that the four *Caenorhabditis* species displayed distinct patterns of H3K9 methylation on X chromosomes prompted us to survey additional related species (Figure 10A). To that end, we examined patterns of H3K9me2 and H3K9me3 in seven additional *Caenorhabditis* species. We found that the X chromosome of males, defined by the absence of H3K4me2, was enriched for either H3K9me2, H3K9me3, or both, in all but one of the species. We also observed that the pattern of H3K9me2/me3 enrichment changed throughout meiotic prophase progression in some species (Figure 10A). Similar patterns were observed on the X chromosome pair of hermaphrodite/female germ cells with some subtle differences between the sexes in the timing of when the repressive mark was loaded and/or removed (Figure S6). While H3K9me2 was the most prevalent mark, we observed no correlation between H3K9me2 enrichment, phylogeny, or sexual mode.

In *C. japonica*, which is the most distantly related species we examined, we observed a distinct pattern. While the *C. japonica* X chromosome in male germ cells was subject to MSCI as monitored by absence of both the activating mark H3K4me2 and Pol2 Ser2-P, we observed neither enrichment for H3K9me2 nor H3K9me3 on the X chromosome (Figure 10, B and C). We did detect enrichment for H3K9me2 on chromosome ends, but this was not specific for the X chromosome. Given the lack of activating marks and transcribing RNA polymerase II, these results suggest that either additional repressive marks are loaded on the X or that another property of the X mediates MSCI in *C. japonica*. Thus, the diverse pattern of chromatin states on the X chromosome among closely related species suggests that the sex chromosome epigenetic state evolves quickly.

Discussion

Here we show that while MSCI is conserved, the epigenetic landscape of sex chromosomes and unpaired genomic regions are distinct in closely related species of *Caenorhabditis*. We also provide evidence for plasticity of the epigenome in mediating diverse functions, including transcription, checkpoint signaling, and DNA replication timing.

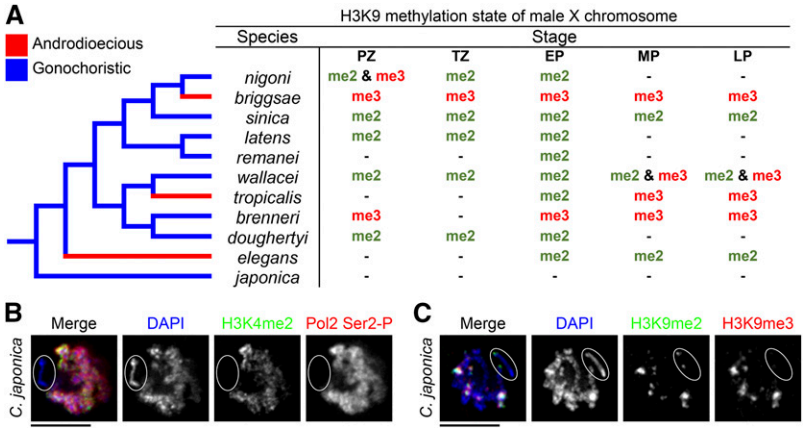

Figure 10 Diverse patterns of X chromosome H3K9 methylation in male germ cells of *Caenorhabditis*. (A) *Caenorhabditis* phylogeny and table showing the H3K9 methylation pattern of the X chromosomes in males of the different species of *Caenorhabditis* through meiotic prophase. EP, early pachytene; MP, midpachytene; LP, late pachytene; PZ, proliferative zone; TZ, transition zone. - indicates the mark is not present. (B) *C. japonica* pachytene nucleus stained with DAPI (blue), anti-H3K4me2 (green), and anti-Pol2 Ser2-P (red). (C) *C. japonica* pachytene nucleus stained with DAPI (blue), anti-H3K9me2 (green), and anti-H3K9me3 (red). X chromosome is circled. Bars, 5 μM.

H3K9me2 vs. H3K9me3

Although H3K9me2 and H3K9me3 are repressive marks that differ only by a single methyl group and are both associated with transcriptional silencing, previous work had suggested that these marks are functionally distinct. In mammals and maize, H3K9me2 has been shown to be associated with facultative heterochromatin, while H3K9me3 has been shown to be associated with constitutive heterochromatin (Peters *et al.* 2003; Rice *et al.* 2003; Shi and Dawe 2006). Our analyses of germ-line chromatin marks in *Caenorhabditis* species indicate that either H3K9me2 or H3K9me3 can be enriched on sex chromosomes and mediate transcriptional silencing, suggesting that these chromatin marks are interchangeable in this context. Based on the definition of Trojer and Reinberg (2007), the X chromosome and unpaired regions represent facultative heterochromatin (*i.e.*, condensed, transcriptionally silent chromatin regions that decondense and allow transcription within temporal, spatial, or parental/heritable context). Thus, at least in *Caernorhabditis* species, these marks do not define facultative *vs.* constitutive heterochromatin.

Why do different H3K9 methylation states mark sex chromosomes/unpaired chromatin in these closely related species? Recent genomic analyses of *Caenorhabditis* species have shown that sexual mode correlates with genome size; hermaphroditic species have 20–40% smaller genomes than obligate female/male species (Fierst *et al.* 2015). However, the particular chromatin mark used for meiotic silencing does not correlate with either sexual mode or genome size. Interestingly, both *C. briggsae* and *C. brenneri*, the two species with enrichment of H3K9me3 on X chromosomes, have a higher content of noncoding repeat sequences compared to *C. elegans* and *C. remanei*, where X chromosomes are enriched for H3K9me2 (Fierst *et al.* 2015). Further, the *C. briggsae* genome has a higher content of transposons, which in mammals are enriched for H3K9me3 (Black and Whetstine 2011). Whether the increase in noncoding/transposon sequences are specifically enriched on the X is not known, but could provide a possible explanation for why *C. briggsae* and *C. brenneri* use H3K9me3 instead of H3K9me2.

In addition to a change in enrichment of H3K9me2 *vs.* H3K9me3 on sequences lacking a pairing partner, analysis of the gene network used for acquisition of H3K9me2/me3 in *C. briggsae* revealed that it is distinct from *C. elegans*. Bessler *et al.* (2010) reported the surprising finding that in the *C. elegans* germ line, H3K9me2 was acquired independently of H3K9me3: *Cel-met-2* mutant germ lines lack H3K9me2 but maintain normal levels of H3K9me3; conversely, *Cel-mes-2* mutant germ lines have normal levels of H3K9me2 and greatly reduced levels of H3K9me3. In contrast to what is observed in *C. elegans*, we found that germ lines from *Cbr-met-2* mutants have severely reduced levels of both H3K9me2 and H3K9me3, suggesting that *Cbr*-MET-2 is responsible for the generation of most germ-line H3K9me2, a subset of which is converted to H3K9me3. Conversion of H3K9me2 to H3K9me3 is most likely mediated by the joint action of *Cbr*-MES-2 and *Cbr*-SET-25, and perhaps additional histone methyltransferases (Figure 4). While MES-2 is important for generation of H3K9me3 in the *C. elegans* germ line (Bessler *et al.* 2010), SET-25 has been shown to be important for acquisition of H3K9me3 in the *C. elegans* embryo (Towbin *et al.* 2012). We found that RNAi inactivation of SET-25 in *C. elegans* results in accumulation of H3K9me2 in the germ line (Figure S4), indicating *Cel*-SET-25 also functions in the germ line as suggested by Ashe *et al.* (2012). Together, these results indicate that the regulatory gene networks that mediate the generation of H3K9me2 and H3K9me3 have diverged between *C. elegans* and *C. briggsae* over the estimated 20–100 million years since their most recent common ancestor (Blair *et al.* 2005; Cutter 2008). This change in the molecular pathway is most likely a consequence of development system drift (DSD) in which processes known to be homologous between taxa (*e.g.*, MSCI) have diverged in their gene regulatory networks (True and Haag 2001). Consistent with this, a recent genome-wide RNAi study indicates that there has been extensive DSD between *C. briggsae* and *C. elegans* (Verster *et al.* 2014).

Our analyses of germ-line H3K9me2 and H3K9me3 patterns in additional *Caenorhabditis* species highlight the speed by which chromatin marks can evolve. While *C. elegans* and

C. briggsae use different H3K9me marks on the X and diverged tens of millions of years ago, *C. briggsae* and *C. nigoni* last shared a common ancestor ~1 million years ago (Cutter 2008; Kiontke *et al.* 2011), yet also have distinct germ-line H3K9me patterns (Figure 10 and Figure S6). Interestingly, these species have different modes of reproduction (*C. briggsae*, androdioecy *vs. C. nigoni*, gonochoristic) but can produce fertile hybrid progeny (Woodruff *et al.* 2010), suggesting that H3K9me2 and H3K9me3 are interchangeable for X chromosome silencing. These findings are also in concordance with functional analyses of the chromatin remodeling NURF complex, where NURF is required for the sperm/oocyte decision in *C. briggsae* but not in *C. nigoni* (Chen *et al.* 2014). Thus, germ-line chromatin marks have the capacity to evolve rapidly.

Why meiotic silencing in Caenorhabditis?

Our analyses of *Caenorhabditis* species germ lines indicate that the process of MSCI is likely to be conserved across the group, suggesting that meiotic silencing is an important property that has been maintained through evolution. This conservation is likely to extend beyond *Caenorhabditis* as cytological analyses suggest that meiotic silencing also occurs in germ cells of *Strongyloides* nematodes (Kulkarni *et al.* 2015). The apparent conservation of MSCI is particularly striking, given the relatively subtle defects that occur when meiotic silencing is disrupted (Bessler *et al.* 2010; Checchi and Engebrecht 2011a; this study). However, as multiple methyltransferases contribute to meiotic silencing, the full functional consequences of disruption of silencing are not currently known.

Many theories have been put forth as to the function of MSCI specifically and meiotic silencing more generally, including facilitating double-strand break repair on unpaired chromatin, activating or silencing meiotic checkpoints and blocking transcription in response to sequences lacking a homologous partner (reviewed in Checchi and Engebrecht 2011b and Turner 2015). In mice, there is very strong evidence that MSCI is critical for silencing a small number of Y-linked genes that when inappropriately expressed, disrupt male meiosis (Royo *et al.* 2010). However, to our knowledge, no X-linked genes have been identified in *Caenorhabditis* that when expressed, are lethal to male meiosis. Indeed, the sex determination mutant *tra-2(lf)*, which transforms XX animals into males with a spermatogenic germ line (Hodgkin and Brenner 1977), progresses through meiosis with normal kinetics, even though the paired Xs are transcriptionally active in late meiotic prophase (Jaramillo-Lambert and Engebrecht 2010). One functional consequence of transcriptional silencing is that genes important for meiosis in general, and spermatogenesis specifically, should be underrepresented on the X chromosome. Consistent with this, transcriptional profiling in *C. elegans* revealed a significant underrepresentation of meiosis and sperm-expressed genes on the X (Reinke *et al.* 2000). It is likely that this underrepresentation of meiosis and spermatogenesis genes is also true of the *Caenorhabditis* group as a whole as there is a high degree of synteny between the X chromosomes in those species with good genomic assemblies (Hillier *et al.* 2007; Fierst *et al.* 2015) and expression analyses have uncovered a depletion of male-biased expressed genes on the X chromosome of *C. briggsae*, *C. remanei*, *C. brenneri*, as well as the more distantly related *Pristionchus pacificus* (Albritton *et al.* 2014).

One surprising feature of meiotic silencing in *Caenorhabditis* is that there are variable and relatively subtle effects on transcription (Checchi and Engebrecht 2011a; Guo *et al.* 2015) (Figure 6 and Figure 7), suggesting that transcriptional silencing does not solely explain the function of MSCI/MSUC. However, additional methyltransferases, as supported by our data, and perhaps other chromatin modifications, contribute to silencing and so the full phenotypic consequence of a failure in meiotic silencing is not known. We do show that in both *C. elegans* and *C. briggsae*, inactivation of MET-2 results in germ-line checkpoint activation, suggesting that checkpoint silencing is an important function for *Caenorhabditis*. Given that sex chromosomes have evolved multiple times, and that MSCI is not conserved throughout metazoa, it is likely that meiotic silencing has evolved differently in different taxa.

Similar to mammals, we observed that meiotic silencing is sensitive to both the dosage of asynapsed chromosomes and presence of constitutively unpaired sex chromosomes. Studies in mice have shown that meiotic silencing is executed efficiently when chromosome asynapsis is low, but excessive amounts of asynapsis are not robustly silenced, and the extent of silencing is dependent on sex, suggesting a limited pool of one or more components of the silencing pathway (Turner *et al.* 2006; Mahadevaiah *et al.* 2008). We show that one limiting factor is the machinery that deposits H3K9me2 and/or H3K9me3 onto asynapsed regions of the genome. Further, we found that the extent of spreading of H3K9me3 and contribution of different histone methyltransferases in the *C. briggsae* germ line is different in hermaphrodites and males. Thus, as with mammals, the extent of meiotic silencing may be an important factor in the sexually dimorphic nature of meiosis.

Uncoupling S phase timing from acquisition of H3K9me2/ me3

Eukaryotic cells have distinct replication programs, whereby different regions of the genome replicate at different times throughout S phase. In general, heterochromatic and H3K9me3-enriched genomic regions replicate late in S phase (Mendez 2009). We found that X chromosomes are late replicating in *C. briggsae* germ cells (Figure 9 and Figure S5) as they are in *C. elegans* (Jaramillo-Lambert *et al.* 2007). Surprisingly, although removal of H3K9me2 and/or H3K9me3 by mutation of MET-2 resulted in transcriptional and checkpoint activation in both species (Figure 5 and Figure 8) (Checchi and Engebrecht 2011a), the X chromosome(s) remained late replicating (Figure 9 and Figure S5). These results suggest that neither H3K9me2 nor H3K9me3 dictate

late replication of the X chromosome (or integrated array) in *Caenorhabditis* germ cells. Interestingly, in the absence of MET-2, H3K4me2 is not loaded (Figure 5) (Checchi and Engebrecht 2011a). Further, *C. elegans* mutants of a small RNA-mediated pathway that disrupt the distribution of H3K9me2 also do not result in accumulation of H3K4me2 on the X (She *et al.* 2009). Thus, it is likely that the chromatin landscape of the X chromosome is still altered, relative to the rest of the genome when H3K9me2/me3 levels are perturbed and this altered epigenome may define late replication in *Caenorhabditis*. In mammals, prereplication complex-associated protein ORCA/LRWD1 has been shown to specifically recruit H3K9 methyltransferases and be important for late replication (Giri *et al.* 2015). However, no orthologs of ORCA/LRWD1 are present in the annotated *Caenorhabditis* genomes. Thus, the mechanisms underlying the replication program in this taxa await future studies.

Conclusion

We show a surprising degree of divergence in the meiotic chromatin landscape across closely related species that share a strikingly similar morphology. These studies suggest that caution be used when considering phenotypes that appear the same among species, as the underlying molecular mechanisms may have changed.

Acknowledgments

We thank Sarit Smolikove for antibodies, Anh Nguyen and Matt Street for constructing RNAi plasmids, and Baptiste Roelens for strains. Many of the strains used in this study were obtained from the *Caenorhabditis* Genetics Center. This work was supported by National Institutes of Health grant GM-103860 and the Agricultural Experimental Station, University of California, Davis, grant CA-D*MCB-7237-H (J.E.).

Literature Cited

Ahmed, S., and J. Hodgkin, 2000 MRT-2 checkpoint protein is required for germline immortality and telomere replication in *C. elegans*. Nature 403: 159–164.

Albritton, S. E., A. L. Kranz, P. Rao, M. Kramer, C. Dieterich *et al.*, 2014 Sex-biased gene expression and evolution of the X chromosome in nematodes. Genetics 197: 865–883.

Andersen, E. C., and H. R. Horvitz, 2007 Two *C. elegans* histone methyltransferases repress *lin-3* EGF transcription to inhibit vulval development. Development 134: 2991–2999.

Ashe, A., A. Sapetschnig, E. M. Weick, J. Mitchell, M. P. Bagijn *et al.*, 2012 piRNAs can trigger a multigenerational epigenetic memory in the germline of *C. elegans*. Cell 150: 88–99.

Bean, C. J., C. E. Schaner, and W. G. Kelly, 2004 Meiotic pairing and imprinted X chromatin assembly in *Caenorhabditis elegans*. Nat. Genet. 36: 100–105.

Bessler, J. B., E. C. Andersen, and A. M. Villeneuve, 2010 Differential localization and independent acquisition of the H3K9me2 and H3K9me3 chromatin modifications in the *Caenorhabditis elegans* adult germ line. PLoS Genet. 6: e1000830.

Bhalla, N., and A. F. Dernburg, 2005 A conserved checkpoint monitors meiotic chromosome synapsis in *Caenorhabditis elegans*. Science 310: 1683–1686.

Black, J. C., and J. R. Whetstine, 2011 Chromatin landscape: methylation beyond transcription. Epigenetics 6: 9–15.

Blair, J. E., P. Shah, and S. B. Hedges, 2005 Evolutionary sequence analysis of complete eukaryote genomes. BMC Bioinformatics 6: 53.

Burgoyne, P. S., S. K. Mahadevaiah, and J. M. Turner, 2009 The consequences of asynapsis for mammalian meiosis. Nat. Rev. Genet. 10: 207–216.

Checchi, P. M., and J. Engebrecht, 2011a *Caenorhabditis elegans* histone methyltransferase MET-2 shields the male X chromosome from checkpoint machinery and mediates meiotic sex chromosome inactivation. PLoS Genet. 7: e1002267.

Checchi, P. M., and J. Engebrecht, 2011b Heteromorphic sex chromosomes: navigating meiosis without a homologous partner. Mol. Reprod. Dev. 78: 623–632.

Checchi, P. M., K. S. Lawrence, M. V. Van, B. J. Larson, and J. Engebrecht, 2014 Pseudosynapsis and decreased stringency of meiotic repair pathway choice on the hemizygous sex chromosome of *Caenorhabditis elegans* males. Genetics 197: 543–560.

Chen, X., F. Xu, C. Zhu, J. Ji, X. Zhou *et al.*, 2014 Dual sgRNA-directed gene knockout using CRISPR/Cas9 technology in *Caenorhabditis elegans*. Sci. Rep. 4: 7581.

Cole, F., S. Keeney, and M. Jasin, 2010 Evolutionary conservation of meiotic DSB proteins: more than just Spo11. Genes Dev. 24: 1201–1207.

Cutter, A. D., 2008 Divergence times in *Caenorhabditis* and *Drosophila* inferred from direct estimates of the neutral mutation rate. Mol. Biol. Evol. 25: 778–786.

de Vries, M., S. Vosters, G. Merkx, K. D'Hauwers, D. G. Wansink *et al.*, 2012 Human male meiotic sex chromosome inactivation. PLoS One 7: e31485.

Dickinson, D. J., J. D. Ward, D. J. Reiner, and B. Goldstein, 2013 Engineering the *Caenorhabditis elegans* genome using Cas9-triggered homologous recombination. Nat. Methods 10: 1028–1034.

Ellis, R. E., and S. Y. Lin, 2014 The evolutionary origins and consequences of self-fertility in nematodes. F1000Prime Rep. 6: 62.

Fierst, J. L., J. H. Willis, C. G. Thomas, W. Wang, R. M. Reynolds *et al.*, 2015 Reproductive mode and the evolution of genome size and structure in *Caenorhabditis* Nematodes. PLoS Genet. 11: e1005323.

Fox, P. M., V. E. Vought, M. Hanazawa, M. H. Lee, E. M. Maine *et al.*, 2011 Cyclin E and CDK-2 regulate proliferative cell fate and cell cycle progression in the *C. elegans* germline. Development 138: 2223–2234.

Fraune, J., M. Alsheimer, J. N. Volff, K. Busch, S. Fraune *et al.*, 2012 Hydra meiosis reveals unexpected conservation of structural synaptonemal complex proteins across metazoans. Proc. Natl. Acad. Sci. USA 109: 16588–16593.

Giri, S., V. Aggarwal, J. Pontis, Z. Shen, A. Chakraborty *et al.*, 2015 The preRC protein ORCA organizes heterochromatin by assembling histone H3 lysine 9 methyltransferases on chromatin. eLife 4: e06496.

Guioli, S., R. Lovell-Badge, and J. M. Turner, 2012 Error-prone ZW pairing and no evidence for meiotic sex chromosome inactivation in the chicken germ line. PLoS Genet. 8: e1002560.

Guo, Y., B. Yang, Y. Li, X. Xu, and E. M. Maine, 2015 Enrichment of H3K9me2 on unsynapsed chromatin in *Caenorhabditis elegans* does not target de novo sites. G3 (Bethesda) 5: 1865–1878.

Handel, M. A., 2004 The XY body: a specialized meiotic chromatin domain. Exp. Cell Res. 296: 57–63.

Hillier, L. W., R. D. Miller, S. E. Baird, A. Chinwalla, L. A. Fulton *et al.*, 2007 Comparison of *C. elegans* and *C. briggsae* genome sequences reveals extensive conservation of chromosome organization and synteny. PLoS Biol. 5: e167.

Hodgkin, J. A., and S. Brenner, 1977 Mutations causing transformation of sexual phenotype in the nematode *Caenorhabditis elegans*. Genetics 86: 275–287.

Holdeman, R., S. Nehrt, and S. Strome, 1998 MES-2, a maternal protein essential for viability of the germline in *Caenorhabditis elegans*, is homologous to a *Drosophila* Polycomb group protein. Development 125: 2457–2467.

Hsin, J. P., and J. L. Manley, 2012 The RNA polymerase II CTD coordinates transcription and RNA processing. Genes Dev. 26: 2119–2137.

Hubbard, E. J., and D. Greenstein, 2005 Introduction to the germ line. WormBook 1: 1–4.

Jaramillo-Lambert, A., and J. Engebrecht, 2010 A single unpaired and transcriptionally silenced X chromosome locally precludes checkpoint signaling in the *Caenorhabditis elegans* germ line. Genetics 184: 613–628.

Jaramillo-Lambert, A., M. Ellefson, A. M. Villeneuve, and J. Engebrecht, 2007 Differential timing of S phases, X chromosome replication, and meiotic prophase in the *C. elegans* germ line. Dev. Biol. 308: 206–221.

Kelly, W. G., C. E. Schaner, A. F. Dernburg, M. H. Lee, S. K. Kim *et al.*, 2002 X-chromosome silencing in the germline of *C. elegans*. Development 129: 479–492.

Kiontke, K., and D. H. Fitch, 2005 The phylogenetic relationships of *Caenorhabditis* and other rhabditids. WormBook 11: 1–11.

Kiontke, K. C., M. A. Felix, M. Ailion, M. V. Rockman, C. Braendle *et al.*, 2011 A phylogeny and molecular barcodes for *Caenorhabditis*, with numerous new species from rotting fruits. BMC Evol. Biol. 11: 339.

Kulkarni, A., J. W. Lightfoot, and A. Streit, 2015 Germline organization in Strongyloides nematodes reveals alternative differentiation and regulation mechanisms. Chromosoma (in press).

Lamelza, P., and N. Bhalla, 2012 Histone methyltransferases MES-4 and MET-1 promote meiotic checkpoint activation in *Caenorhabditis elegans*. PLoS Genet. 8: e1003089.

Liu, Q., S. Guntuku, X. S. Cui, S. Matsuoka, D. Cortez *et al.*, 2000 Chk1 is an essential kinase that is regulated by Atr and required for the G(2)/M DNA damage checkpoint. Genes Dev. 14: 1448–1459.

Lui, D. Y., and M. P. Colaiacovo, 2013 Meiotic development in *Caenorhabditis elegans*. Adv. Exp. Med. Biol. 757: 133–170.

Mahadevaiah, S. K., D. Bourc'his, D. G. de Rooij, T. H. Bestor, J. M. Turner *et al.*, 2008 Extensive meiotic asynapsis in mice antagonises meiotic silencing of unsynapsed chromatin and consequently disrupts meiotic sex chromosome inactivation. J. Cell Biol. 182: 263–276.

Maine, E. M., J. Hauth, T. Ratliff, V. E. Vought, X. She *et al.*, 2005 EGO-1, a putative RNA-dependent RNA polymerase, is required for heterochromatin assembly on unpaired dna during *C. elegans* meiosis. Curr. Biol. 15: 1972–1978.

Meiklejohn, C. D., E. L. Landeen, J. M. Cook, S. B. Kingan, and D. C. Presgraves, 2011 Sex chromosome-specific regulation in the *Drosophila* male germline but little evidence for chromosomal dosage compensation or meiotic inactivation. PLoS Biol. 9: e1001126.

Mendez, J., 2009 Temporal regulation of DNA replication in mammalian cells. Crit. Rev. Biochem. Mol. Biol. 44: 343–351.

Mikhaylova, L. M., and D. I. Nurminsky, 2011 Lack of global meiotic sex chromosome inactivation, and paucity of tissue-specific gene expression on the *Drosophila* X chromosome. BMC Biol. 9: 29.

Mlynarczyk-Evans, S., B. Roelens, and A. M. Villeneuve, 2013 Evidence that masking of synapsis imperfections counterbalances quality control to promote efficient meiosis. PLoS Genet. 9: e1003963.

Morelli, M. A., and P. E. Cohen, 2005 Not all germ cells are created equal: aspects of sexual dimorphism in mammalian meiosis. Reproduction 130: 761–781.

Nuez, I., and M. A. Felix, 2012 Evolution of susceptibility to ingested double-stranded RNAs in *Caenorhabditis* nematodes. PLoS One 7: e29811.

Peters, A. H., S. Kubicek, K. Mechtler, R. J. O'Sullivan, A. A. Derijck *et al.*, 2003 Partitioning and plasticity of repressive histone methylation states in mammalian chromatin. Mol. Cell 12: 1577–1589.

Phillips, C. M., and A. F. Dernburg, 2006 A family of zinc-finger proteins is required for chromosome-specific pairing and synapsis during meiosis in *C. elegans*. Dev. Cell 11: 817–829.

Phillips, C. M., C. Wong, N. Bhalla, P. M. Carlton, P. Weiser *et al.*, 2005 HIM-8 binds to the X chromosome pairing center and mediates chromosome-specific meiotic synapsis. Cell 123: 1051–1063.

Reinke, V., H. E. Smith, J. Nance, J. Wang, C. Van Doren *et al.*, 2000 A global profile of germline gene expression in *C. elegans*. Mol. Cell 6: 605–616.

Reuben, M., and R. Lin, 2002 Germline X chromosomes exhibit contrasting patterns of histone H3 methylation in *Caenorhabditis elegans*. Dev. Biol. 245: 71–82.

Rice, J. C., S. D. Briggs, B. Ueberheide, C. M. Barber, J. Shabanowitz *et al.*, 2003 Histone methyltransferases direct different degrees of methylation to define distinct chromatin domains. Mol. Cell 12: 1591–1598.

Royo, H., G. Polikiewicz, S. K. Mahadevaiah, H. Prosser, M. Mitchell *et al.*, 2010 Evidence that meiotic sex chromosome inactivation is essential for male fertility. Curr. Biol. 20: 2117–2123.

Schimenti, J., 2005 Synapsis or silence. Nat. Genet. 37: 11–13.

Shakes, D. C., J. C. Wu, P. L. Sadler, K. Laprade, L. L. Moore *et al.*, 2009 Spermatogenesis-specific features of the meiotic program in *Caenorhabditis elegans*. PLoS Genet. 5: e1000611.

She, X., X. Xu, A. Fedotov, W. G. Kelly, and E. M. Maine, 2009 Regulation of heterochromatin assembly on unpaired chromosomes during *Caenorhabditis elegans* meiosis by components of a small RNA-mediated pathway. PLoS Genet. 5: e1000624.

Shi, J., and R. K. Dawe, 2006 Partitioning of the maize epigenome by the number of methyl groups on histone H3 lysines 9 and 27. Genetics 173: 1571–1583.

Timmons, L., D. L. Court, and A. Fire, 2001 Ingestion of bacterially expressed dsRNAs can produce specific and potent genetic interference in *Caenorhabditis elegans*. Gene 263: 103–112.

Towbin, B. D., C. Gonzalez-Aguilera, R. Sack, D. Gaidatzis, V. Kalck *et al.*, 2012 Step-wise methylation of histone H3K9 positions heterochromatin at the nuclear periphery. Cell 150: 934–947.

Trojer, P., and D. Reinberg, 2007 Facultative heterochromatin: Is there a distinctive molecular signature? Mol. Cell 28: 1–13.

True, J. R., and E. S. Haag, 2001 Developmental system drift and flexibility in evolutionary trajectories. Evol. Dev. 3: 109–119.

Turner, J. M., 2007 Meiotic sex chromosome inactivation. Development 134: 1823–1831.

Turner, J. M., 2015 Meiotic silencing in mammals. Annu. Rev. Genet. 49: 395–412.

Turner, J. M., O. Aprelikova, X. Xu, R. Wang, S. Kim *et al.*, 2004 BRCA1, histone H2AX phosphorylation, and male meiotic sex chromosome inactivation. Curr. Biol. 14: 2135–2142.

Turner, J. M., S. K. Mahadevaiah, O. Fernandez-Capetillo, A. Nussenzweig, X. Xu *et al.*, 2005 Silencing of unsynapsed meiotic chromosomes in the mouse. Nat. Genet. 37: 41–47.

Turner, J. M., S. K. Mahadevaiah, P. J. Ellis, M. J. Mitchell, and P. S. Burgoyne, 2006 Pachytene asynapsis drives meiotic sex chromosome inactivation and leads to substantial postmeiotic repression in spermatids. Dev. Cell 10: 521–529.

van der Heijden, G. W., A. A. Derijck, E. Posfai, M. Giele, P. Pelczar *et al.*, 2007 Chromosome-wide nucleosome replacement and H3.3 incorporation during mammalian meiotic sex chromosome inactivation. Nat. Genet. 39: 251–258.

Verster, A. J., A. K. Ramani, S. J. McKay, and A. G. Fraser, 2014 Comparative RNAi screens in *C. elegans* and *C. briggsae* reveal the impact of developmental system drift on gene function. PLoS Genet. 10: e1004077.

Vibranovski, M. D., 2014 Meiotic sex chromosome inactivation in *Drosophila*. J. Genomics 2: 104–117.

Vibranovski, M. D., H. F. Lopes, T. L. Karr, and M. Long, 2009 Stage-specific expression profiling of *Drosophila* spermatogenesis suggests that meiotic sex chromosome inactivation drives genomic relocation of testis-expressed genes. PLoS Genet. 5: e1000731.

Villeneuve, A. M., and K. J. Hillers, 2001 Whence meiosis? Cell 106: 647–650.

Woodruff, C. C., O. Eke, S. E. Baird, M. A. Felix, and E. S. Haag, 2010 Insights into species divergence and the evolution of hermaphroditism from fertile interspecies hybrids of *Caenorhabditis* nematodes. Genetics 186: 997–1012.

Xiao, B., J. R. Wilson, and S. J. Gamblin, 2003 Domains and histone methylation. Curr. Opin. Struct. Biol. 13: 699–705.

Zickler, D., and N. Kleckner, 2015 Recombination, pairing, and synapsis of homologs during meiosis. Cold Spring Harb. Perspect. Biol. 7: a016626.

Communicating editor: M. P. Colaiacovo

GENETICS

Supporting Information
www.genetics.org/lookup/suppl/doi:10.1534/genetics.116.191130/-/DC1

Plasticity in the Meiotic Epigenetic Landscape of Sex Chromosomes in *Caenorhabditis* Species

Braden J. Larson, Mike V. Van, Taylor Nakayama, and JoAnne Engebrecht

DOI: 10.1534/genetics.116.191130

A

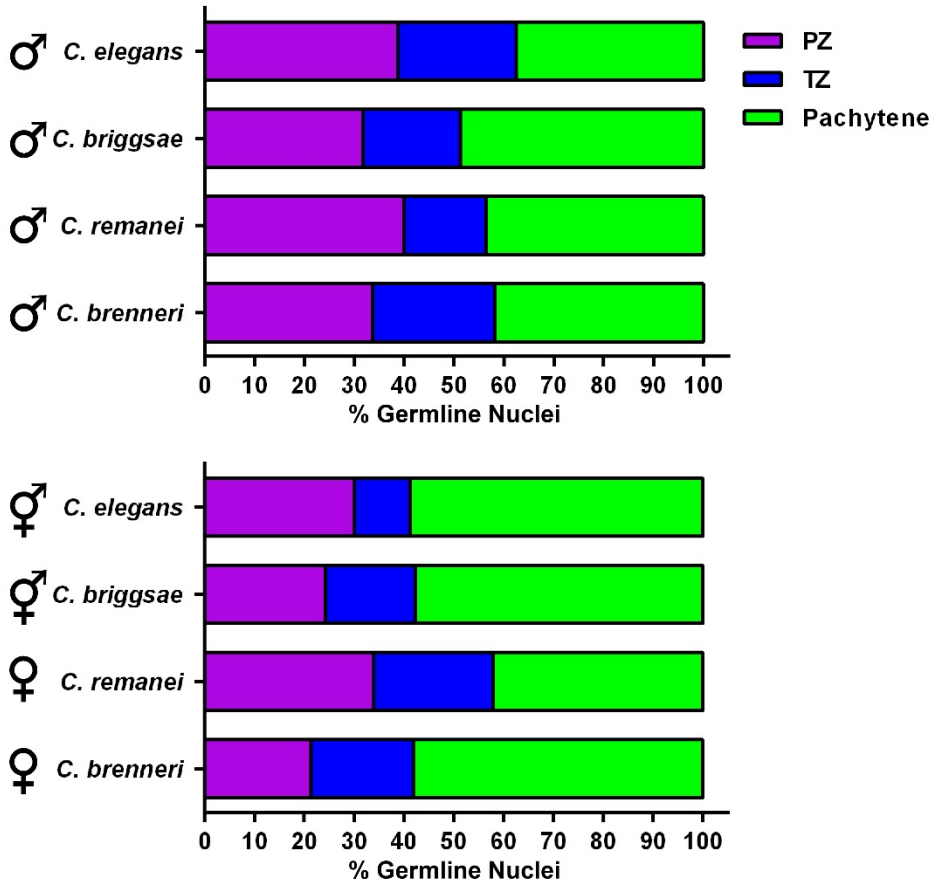

B

Average Number of Nuclei per Stage of the Germ Line

		PZ		TZ		Pachytene	
Species	**n**	Avg.	SEM	Avg.	SEM	Avg.	SEM
♂ *C. elegans*	3	183.0	7.6	113.3	9.1	179.7	21.2
♂ *C. briggsae*	3	99	1.53	61	2.52	154.7	20.7
♂ *C. remanei*	4	100	2.97	40.75	1.03	110	9.43
♂ *C. brenneri*	4	96.75	8.05	70.5	7.27	119.5	6.84
⚥ *C. elegans*	3	228.7	29.1	85.67	6.06	446	62.98
⚥ *C. briggsae*	3	121	12.5	90.33	2.3	287.7	30.15
♀ *C. remanei*	4	172.5	11.5	121	18.4	214	26.2
♀ *C. brenneri*	4	88.75	5.8	85.5	8.29	241.8	35.83

Figure S1. Quantification of the number of germ line nuclei per stage in different *Caenorhabditis* species

(A) Percent of total nuclei per stage of the germ line. (**B**) Raw scores of average nuclei per stage of the germ line.

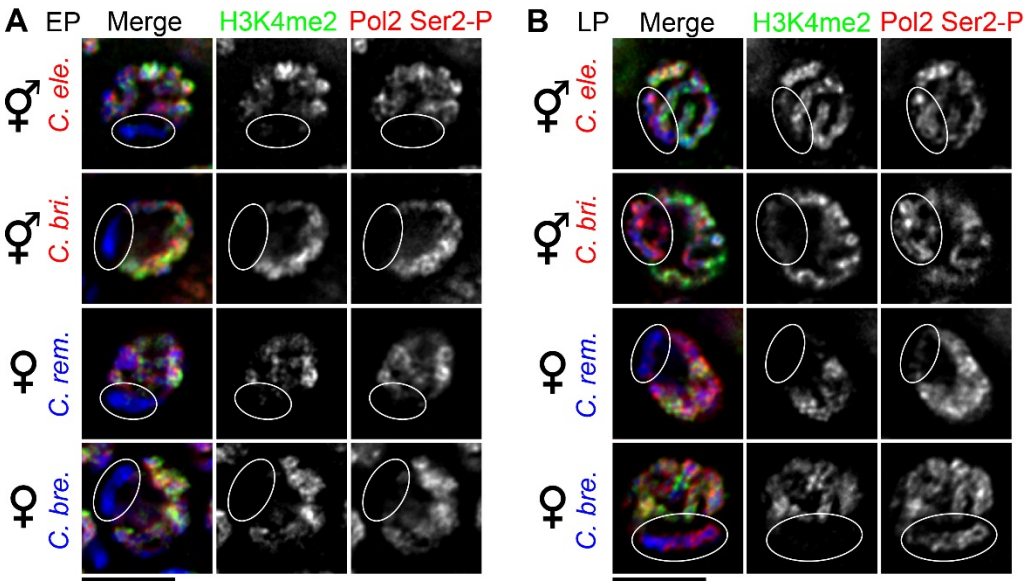

Figure S2. H3K4me2 and Pol2 Ser2-P patterns in Hermaphrodites/ Females
C. elegans, *C. briggsae*, *C. remanei*, and *C. brenneri* early pachytene nuclei stained with DAPI (blue), anti-H3K4me2 (green), and anti-RNA Pol2 Ser2-P (red). (**A**) In early pachytene (EP) both the promotive chromatin mark H3K4me2 and actively transcribing RNA polymerase (Pol2 Ser2-P) were largely absent from the paired X chromosomes of hermaphrodites/females (circled). (**B**) By late pachytene (LP) Pol2 Ser2-P and variable amounts of H3K4me2 colocalized with the paired X chromosomes. Scale Bars = 5 μM.

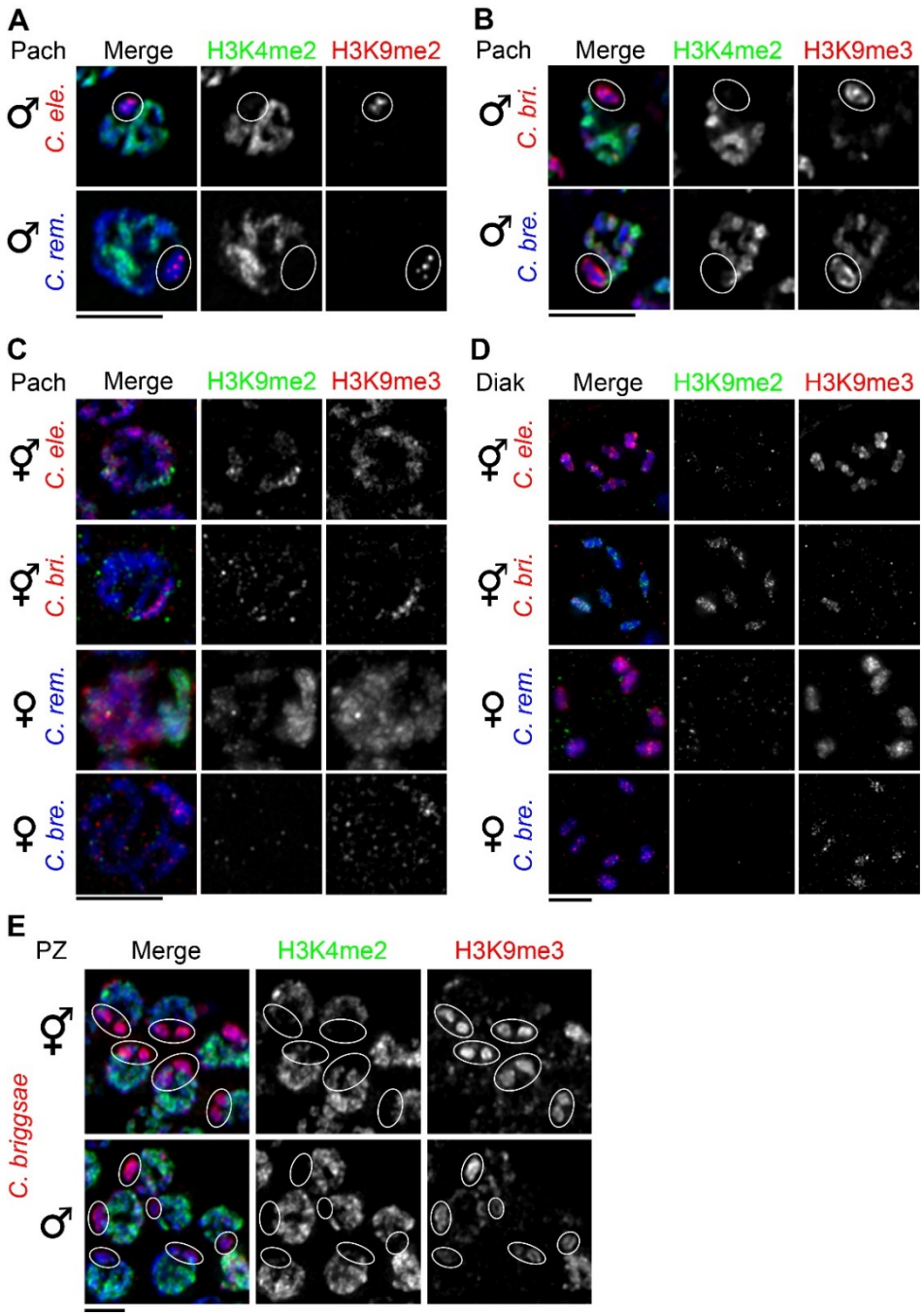

Figure S3. Chromatin marks on the X chromosome of *Caenorhabditis* species.
(A) *C. elegans* and *C. remanei* male pachytene nuclei stained with DAPI (blue), anti-H3K4me2 (green), and anti-H3K9me2 (red). **(B)** *C. briggsae*, and *C. brenneri* male pachytene nuclei stained with DAPI (blue), anti-H3K4me2 (green), and anti-H3K9me3 (red). **(C)** *C. elegans*, *C. briggsae*, *C. remanei,* and *C. brenneri* hermaphrodite/female pachytene nuclei stained with DAPI (blue), anti-H3K9me2 (green), and anti-H3K9me3 (red). **(D)** *C. elegans*, *C. briggsae*, *C. remanei* and *C. brenneri* hermaphrodite/female diakinesis nuclei stained with DAPI (blue), anti-H3K9me2 (green), and anti-H3K9me2 (red). **(E)** *C. briggsae* proliferative zone nuclei stained with DAPI (blue), anti-H3K4me2 (green), and anti-H3K9me3 (red). Circles indicate the X chromosome(s). All scale bars = 5 μM.

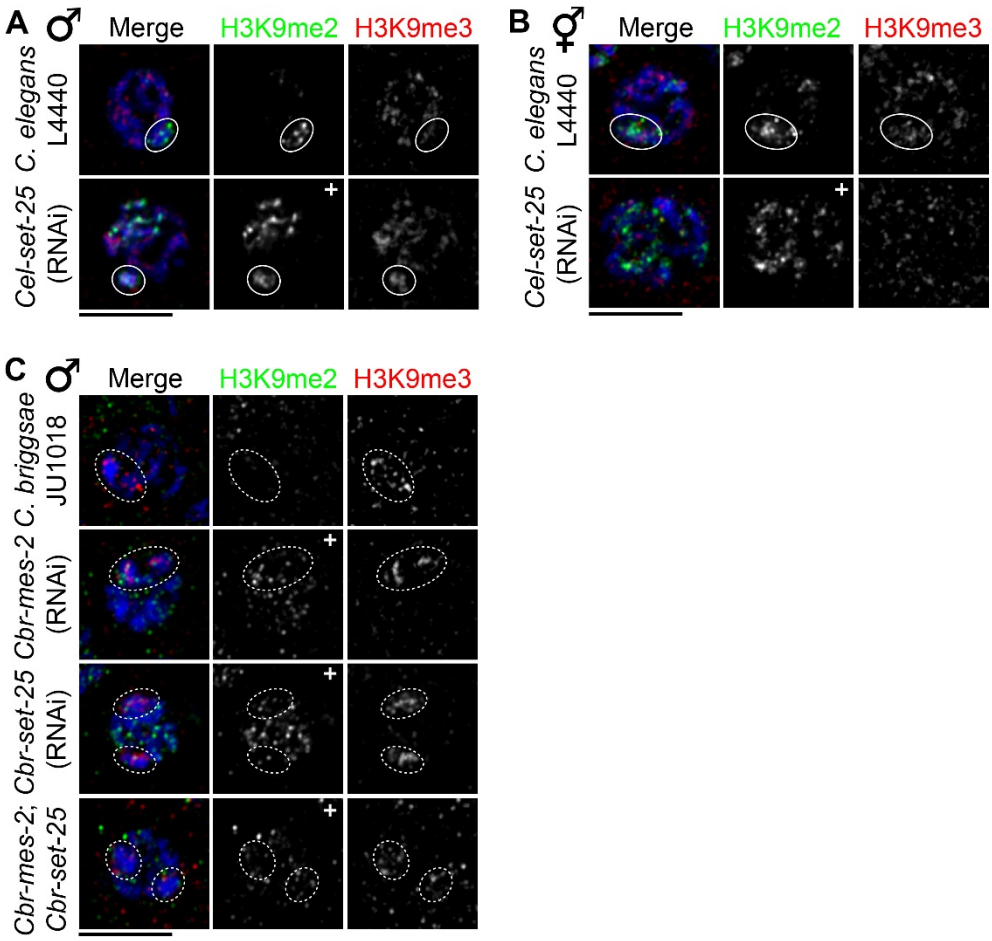

Figure S4. MES-2 and SET-25 methylate H3K9me2 to H3K9me3 in *C. elegans* and *C. briggsae* germ lines

(A,B) *C. elegans* pachytene nuclei stained with DAPI (blue), anti-H3K9me2 (green), and anti-H3K9me3 (red) from Male **(A)** and hermaphrodite **(B)** germ lines of the indicated genotypes. (+) indicate ectopic signal in the panel. **(C)** Male *C. briggsae* early pachytene nuclei stained with DAPI (blue), anti-H3K9me2 (green), and anti-H3K9me3 (red). *Cbr-mes-2*, *Cbr-set-25* and *Cbr-mes-2; Cbr-set-25* RNAi treated worms have similar amounts of ectopic H3K9me2 at early pachytene (+). Dotted circles indicate either the X chromosome and/or integrated transgene array. Scale Bars = 5 µM.

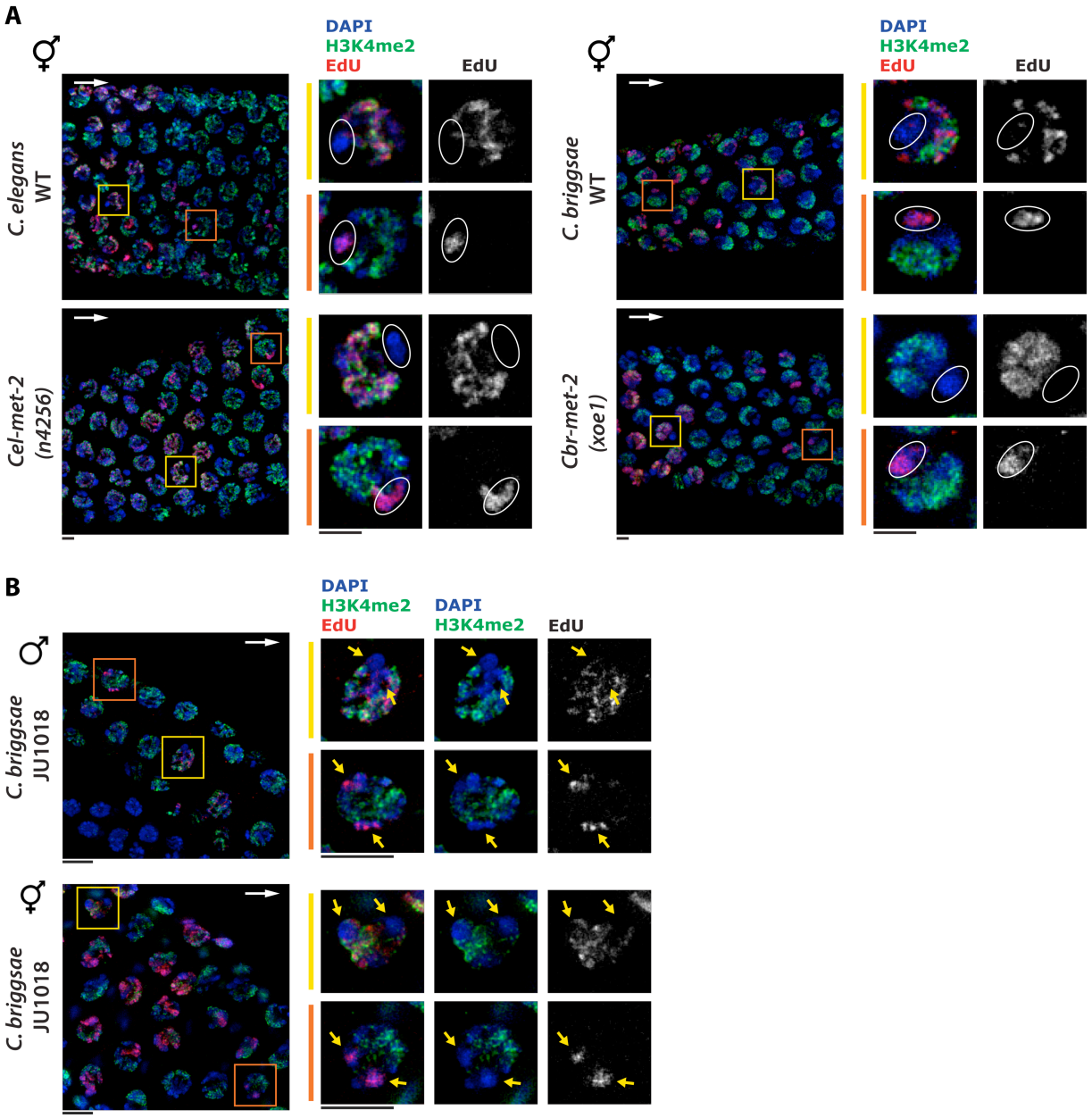

Figure S5. Late Replication of the X chromosomes in germline S-phases is not dependent on MET-2 in *C. elegans* and *C. briggsae* hermaphrodites

(**A**) *C. elegans* and *C. briggsae* EdU (red) labeled pachytene nuclei stained with DAPI (blue) and anti-H3K4me2 (green). White arrow indicates direction of meiotic progression; X chromosomes are circled. Examples of nuclei early and late in S phase are marked by yellow and orange boxes/lines, respectively. Scale Bars = 2 μM. (**B**) Integrated array and X chromosomes have a common property that dictates late replication. *C. briggsae* JU1018 male and hermaphrodite nuclei labeled with EdU (red) and stained with DAPI (blue) and anti-H3K4me2 (green). Yellow arrows point to the sex chromosomes and chromosome V with integrated array which was identified by the absence of H3K4me2. Scale Bars = 5 μM.

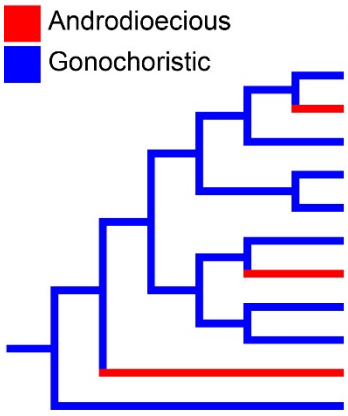

Species	H3K9 methylation state of female/hermaphrodite X chromosome: Stage				
	PZ	TZ	EP	MP	LP
nigoni	me2 & me3	me2	me2	me2	me2
briggsae	me3	me3	me3	me3	me3
sinica	-	me2	me2	me2	me2
latens	me2	me2	me2	me2	me3
remanei	-	-	me2	me2	-
wallacei	me2 & me3	me2	me2	me2	me2
tropicalis	me3	-	me2	me3	me3
brenneri	me3	me3	me3	me3	me3
doughertyi	me2	me2	me2	me2	me2
elegans	-	-	me2	me2	me2
japonica	-	-	-	-	-

Figure S6. Diverse patterns of X chromosomes H3K9 methylation in hermaphrodite/female germ cells of *Caenorhabditis*

Caenorhabditis phylogeny and table showing the H3K9 methylation state of female/hermaphrodite X chromosomes in different species of *Caenorhabditis* through meiotic prophase. PZ, proliferative zone; TZ, transition zone; EP, early pachytene; MP, mid-pachytene; LP, late pachytene. (–) indicates the mark is not present.

Table S1. Primer sequences used to construct *C. briggsae* RNAi feeding vectors by restriction cloning or two piece Gibson assembly.

Name	**Sequence**
Cbr-met-2 forward (p1058)	TTC CCC TAC AAC GCC AGT GT
Cbr-met-2 reverse (p1059)	TGC TGG ACG ACG CAA TTT GG
Cbr-mes-2 Forward L4440	AATTCGAGCTCCACCGCGGTTTCCTCTTCCGATGATCGTGAC
Cbr-mes-2 reverse L4440	CTAGTTCTAGAGCGGCCGCCCACCATCTCCCATCAAACTTCA
L4440 Forward *Cbr-mes-2*	GTCACGATCATCGGAAGAGGAAACCGCGGTGGAGCTCGAATT
L4440 Reverse *Cbr-mes-2*	TGAAGTTTGATGGGAGATGGTGGGCGGCCGCTCTAGAACTAG
Cbr-set-25 Forward L4440	AATTCGAGCTCCACCGCGGTTCGACGTTGTTTTCAGGCCA
Cbr-set-25 reverse L4440	CTAGTTCTAGAGCGGCCGCCGGGATTTCATCGTTACTGCCG
L4440 Forward *Cbr-set-25*	CGGCAGTAACGATGAAATCCCGGCGGCCGCTCTAGAACTAG
L4440 Reverse *Cbr-set-25*	TGGCCTGAAAACAACGTCGAACCGCGGTGGAGCTCGAATT
Cbr-him-8 Forward L4440	AATTCGAGCTCCACCGCGGTTGCAATTTAGAAGTTCCGCG
Cbr-him-8 reverse L4440	CTAGTTCTAGAGCGGCCGCCGGATAGGAATTGTAATCTCGC
L4440 Forward *Cbr-him-8*	GCGAGATTACAATTCCTATCCGGCGGCCGCTCTAGAACTAG
L4440 Reverse *Cbr-him-8*	CGCGGAACTTCTAAATTGCAACCGCGGTGGAGCTCGAATT
Cbr-zim-1 Forward L4440	AATTCGAGCTCCACCGCGGTGACTTGCGACGAGTGGAACA
Cbr-zim-1 Reverse L4440	CTAGTTCTAGAGCGGCCGCCGGAGCGGTATTCGCCGATGT
L4440 Forward *Cbr-zim-1*	ACATCGGCGAATACCGCTCCGGCGGCCGCTCTAGAACTAG
L4440 Reverse *Cbr-zim-1*	TGTTCCACTCGTCGCAAGTCACCGCGGTGGAGCTCGAATT
Cbr-zim-2 Forward L4440	AATTCGAGCTCCACCGCGGTGGAGTGGTCCTGGAGACAGT
Cbr-zim-2 reverse L4440	CTAGTTCTAGAGCGGCCGCCTGCATCTCCTTTCACTTGGCT
L4440 Forward *Cbr-zim-2*	AGCCAAGTGAAAGGAGATGCAGGCGGCCGCTCTAGAACTAG
L4440 Reverse *Cbr-zim-2*	ACTGTCTCCAGGACCACTCCACCGCGGTGGAGCTCGAATT
Cbr-chk-1 Forward L4440	AATTCGAGCTCCACCGCGGTCTACCGATTCCCACAGCACC
Cbr-chk-1 Reverse L4440	CTAGTTCTAGAGCGGCCGCCCCAGCCATTGAAGGTAAGCG
L4440 Forward *Cbr-chk-1*	CGCTTACCTTCAATGGCTGGGGCGGCCGCTCTAGAACTAG
L4440 Reverse *Cbr-chk-1*	GGTGCTGTGGGAATCGGTAGACCGCGGTGGAGCTCGAATT